Discontinuous codimension-two bifurcation in a Vlasov equation

Yoshiyuki Y. Yamaguchi
Graduate School of Informatics, Kyoto University, Kyoto 606-8501, Japan

Julien Barré
Institut Denis Poisson, Université d'Orléans, Université de Tours and CNRS, 45067 Orléans, France

(Received 5 December 2022; accepted 1 April 2023; published 2 May 2023)

In a Vlasov equation, the destabilization of a homogeneous stationary state is typically described by a continuous bifurcation characterized by strong resonances between the unstable mode and the continuous spectrum. However, when the reference stationary state has a flat top, it is known that resonances drastically weaken and the bifurcation becomes discontinuous. In this article we analyze one-dimensional spatially periodic Vlasov systems, using a combination of analytical tools and precise numerical simulations to demonstrate that this behavior is related to a codimension-two bifurcation, which we study in detail.

DOI: 10.1103/PhysRevE.107.054203

I. INTRODUCTION

Vlasov and other similar equations are infinite-dimensional Hamiltonian systems (see, for instance, [1]) which are fundamental in many domains governed by long-range interactions, for instance, plasma physics, astrophysics, and fluid dynamics. Getting a qualitative understanding of Vlasov dynamics is thus an old problem, which started with Vlasov and Landau [2,3]. We approach this question with dynamical systems tools, in particular bifurcation theory; the rationale is that bifurcations have a universal character and tend to provide information on the structure of the phase space, in a sometimes rather wide neighborhood of the critical point.

The bifurcation theory of Vlasov and Vlasov-like equations is very different from that of dissipative nonlinear partial differential equations (PDEs). The paradigmatic case for a bifurcation of the Vlasov equation is a homogeneous stationary solution with a certain velocity profile $F(p)$ which becomes unstable as a parameter (a coupling constant, for instance) is varied. This situation is now well understood: The unstable eigenvalue appears embedded in the marginally stable (purely imaginary) continuous spectrum, and a reduced description involving a finite-dimensional central manifold is not possible. Instead, the development and saturation of the instability is generically described by the single-wave model, which is itself a nonlinear PDE [4–7]. In particular, the bifurcation is continuous, and if λ is a real eigenvalue and indicates the instability rate, the nonlinear saturation amplitude of the instability is the peculiar $O(\lambda^2)$ trapping scaling rather than the much larger $O(\lambda^{1/2})$ typical for standard pitchfork bifurcations [8,9] in dissipative systems.

Beyond this generic scenario, it is also well known that modifying the velocity profile of the stationary state may have a strong influence on the type of bifurcation: Indeed, for flat-top velocity profiles, or water bags, resonance effects between the unstable mode and the continuous spectrum are suppressed and the validity of the standard central manifold approach is recovered; a finite-dimensional reduction is then achievable and in all cases in which the computation has been attempted it predicts a discontinuous bifurcation [7,10].

At the critical point, a purely imaginary eigenvalue λ_I appears; this requires the first derivative of the velocity profile to vanish at λ_I: $F'(\lambda_I) = 0$. The generic scenario then corresponds to $F''(\lambda_I) \neq 0$ and the flat-top case to the vanishing of all derivatives: $F^{(n)}(\lambda_I) = 0$ for any $n \in \mathbb{N}$. In the review in [7] (see Sec. VIII-C therein) the authors numerically analyze, in the simple setting of the Hamiltonian mean-field model, how the standard single-wave model bifurcation is modified when the critical velocity profile interpolates between a Gaussian and a water bag. We undertake in this article a systematic study of this situation and show that it can be understood as the influence of a special point in the family of single-wave model bifurcations, i.e., a kind of codimension-two bifurcation, which rules the dynamics in its neighborhood.

A typical example of codimension-two bifurcation is the Bogdanov-Takens bifurcation in a dissipative ordinary differential equation [11]. Another physically important example is a tricritical point in thermodynamics; such a tricritical point has also been observed in a Vlasov system [12] in relation to Lynden-Bell statistical mechanics. At variance with [12], which uses nonstationary water-bag initial states, we consider in the present work small perturbations of smooth stationary reference states. Beyond the case of homogeneous states, bifurcations of Vlasov equations have also been studied for families of nonhomogeneous (position depending) distributions, in the context of self-gravitating systems [13], and more recently in [14,15]; these studies are restricted however to codimension-one bifurcations.

To be more precise, for simplicity we restrict our discussion to one-dimensional Vlasov equations with periodic boundary condition and to even velocity profiles. We consider a family F_α of stationary states parametrized by α, which are unimodal for $\alpha \leqslant 0$ and bimodal for $\alpha > 0$. A coupling constant provides one more tunable parameter, which induces instability of the reference state, and a codimension-two bifurcation lies on the line $\alpha = 0$. The existence of a critical

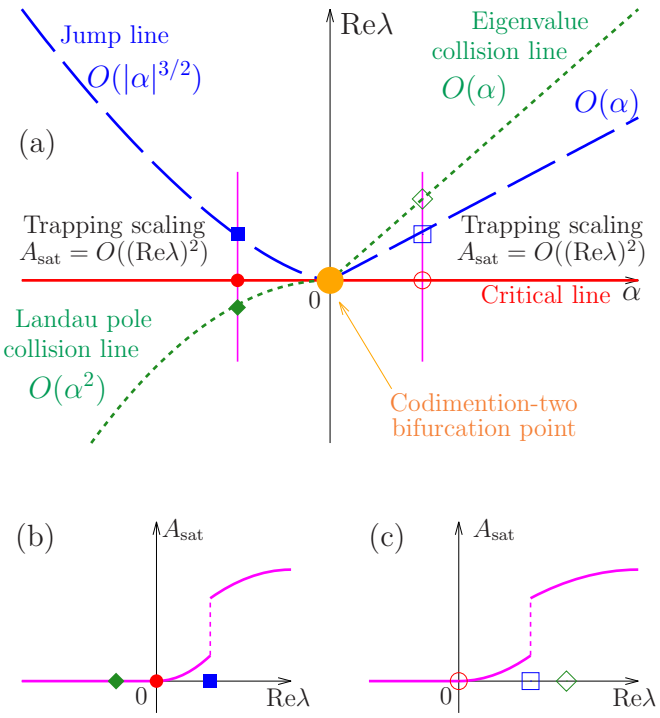

FIG. 1. (a) Sketch of the two-dimensional parameter space $(\alpha, \mathrm{Re}\lambda)$, where α parametrizes a family of reference stationary states F_α: F_α is unimodal for $\alpha \leqslant 0$ and bimodal for $\alpha > 0$. Here λ is the eigenvalue or Landau pole which has the largest real part. The codimension-two bifurcation point is the origin $(\alpha, \mathrm{Re}\lambda) = (0, 0)$. The three types of lines are the critical line (red solid), the eigenvalue collision line (green dotted), and the jump line (blue dashed). Trapping scaling $A_{\rm sat} = O((\mathrm{Re}\lambda)^2)$ appears between the critical line and the jump line, where $A_{\rm sat}$ is the asymptotically saturated amplitude of the unstable mode. (b) Sketch of a curve representing $A_{\rm sat}$ as a function of $\mathrm{Re}\lambda$, along the left magenta vertical line in (a). (c) Same as (b) but along the right magenta vertical line. In both cases (b) and (c) the bifurcation is continuous with trapping scaling, but the asymptotic amplitude then shows a jump. In (b) [(c)], Landau damping (instability) is oscillatory to the left of the green diamond point and nonoscillatory to the right.

unimodal velocity profile requires the interaction to be attractive, which we assume in the following. A typical example is provided by self-gravitating systems and another remarkable example is a system consisting of trapped ions, whose interaction range can be experimentally controlled from short to long [16–20].

Our results are schematically illustrated on Fig. 1. We first analyze the codimension-two bifurcation at the linear level, showing that it is characterized by a collision of two complex conjugate eigenvalues (or Landau poles) λ and λ^* on the real axis. We call this, in the following, eigenvalue collision; it should not be confused with the points where one or two eigenvalues cross the imaginary axis: At these points the reference state becomes unstable and we call them critical points. For simplicity, when Landau poles (and not bona fide eigenvalues) collide on the real axis, we also call it an eigenvalue collision. At the codimension-two point, which we also call a bifurcation point, the eigenvalue collision happens exactly for $\lambda = 0$, at the same time as the critical point.

In the neighborhood of the bifurcation point, Landau poles are close to the imaginary axis and not always real: Landau damping is then weak and may be oscillating. As a standard central manifold expansion is in general not valid in this case, we use a combination of complementary methods to study the bifurcation at the nonlinear level.

(i) The self-consistent equation [21–25] focuses on computing approximately the asymptotic stationary state after the nonlinear evolution of the instability. It predicts a discontinuous transition at the codimension-two bifurcation point; in the unimodal region $\alpha < 0$, it predicts a continuous bifurcation, followed, deeper in the unstable region, by a discontinuous jump of the asymptotic state. However, the self-consistent equation is not applicable for the bimodal region $\alpha > 0$ close to the tricritical point $\alpha = 0$.

(ii) Direct numerical simulations confirm the analytical results when they are available and allow us to explore the regimes when they are not. Numerical simulations reveal in particular that the bifurcation is always continuous except at the codimension-two bifurcation point, but that this continuous bifurcation is followed by a jump of the asymptotic state in the bimodal side $\alpha > 0$ as well as the unimodal side $\alpha < 0$. The region where the bifurcation is continuous, which is described by trapping scaling and the single-wave model, drastically shrinks when we approach the codimension-two bifurcation point from either side, vanishing at the bifurcation point. We also complement our analysis by studying the case of more vanishing derivatives of the critical profile F_0.

The rest of the paper is organized to explain Fig. 1 as follows. We present the model and the corresponding Vlasov equation in more detail in Sec. II. We develop the linear theory of the bifurcation in Sec. III. The linear theory in particular derives the eigenvalue collision point, which plays an essential role in understanding the jump in the bimodal case ($\alpha > 0$). A nonlinear theory is developed in Sec. IV and used to analyze in detail the unimodal case ($\alpha \leqslant 0$), including the jump line following the continuous bifurcation. Direct numerical simulations of the Vlasov equation in Sec. V provide comparisons and complements for these theoretical predictions.

II. MODEL

We consider a spatially one-dimensional system with periodic boundary condition. The N-body Hamiltonian is

$$H_N = \sum_{i=1}^{N} \frac{p_i^2}{2} + \frac{1}{2N} \sum_{i=1}^{N} \sum_{j=1}^{N} \phi(q_i - q_j), \tag{1}$$

where $\phi(q)$ is a 2π-periodic and even coupling function. The coupling function is then expanded in a Fourier series as

$$\phi(q) = -\sum_{k=1}^{\infty} K_k \cos(kq), \tag{2}$$

where the constant term ($k = 0$) is omitted. A positive coefficient $K_k > 0$ means that the kth Fourier mode generates an attractive interaction, which may destabilize the homogeneous state. If $K_1 = 1$ and $K_k = 0$ ($k > 1$), the N-body system is called the Hamiltonian mean-field (HMF) model [26,27],

which is a paradigmatic mean-field model. We assume that

$$K_1 > |K_k| \quad (k > 1) \tag{3}$$

so that the instability occurs in the first Fourier mode. We use K_1 as the first bifurcation parameter corresponding to λ in Fig. 1 and rename it K for simplicity: The homogeneous state is stable for small K and unstable for large K.

The mean-field-like interaction in (1) allows us to describe dynamics of the N-body system in the limit $N \to \infty$ by the Vlasov equation [28–30]

$$\frac{\partial f}{\partial t} + \frac{\partial H[f]}{\partial p}\frac{\partial f}{\partial q} - \frac{\partial H[f]}{\partial q}\frac{\partial f}{\partial p} = 0. \tag{4}$$

Here $f(q, p, t)$ is the one-particle distribution function with the normalization condition

$$\iint_\mu f(q, p, t) dq\, dp = 1 \tag{5}$$

and $H[f](q, p, t)$ is the one-particle Hamiltonian functional defined by

$$H[f](q, p, t) = \frac{p^2}{2} + \iint_\mu \phi(q - q') f(q', p', t) dq' dp', \tag{6}$$

where μ is the one-particle phase space spanned by the position variable $q \in (-\pi, \pi]$ and the conjugate momentum variable $p \in \mathbb{R}$.

We recall three important facts about the Vlasov equation. First, any homogeneous distribution, which depends on p only, is a stationary solution to the Vlasov equation (4). Second, the Vlasov equation has an infinite number of conserved quantities, called Casimir invariants, irrespective of the Hamiltonian. A Casimir invariant is of the form

$$\mathcal{C}[f] = \iint_\mu c(f(q, p)) dq\, dp, \tag{7}$$

where c is an arbitrary smooth function (see, for instance, Ref. [31], Pt. III). Third, from the condition (3), the stability of a homogeneous stationary state $F(p)$ is obtained from the spectral function for the first Fourier mode $\Lambda_1(\lambda)$, where the spectral function for the kth Fourier mode is (see [32], or [33] in the context of self-gravitating systems)

$$\Lambda_k(\lambda) = 1 + K_k \pi \int_{\mathbb{R}} \frac{F^{(1)}(p)}{p - i\lambda/k} dp. \tag{8}$$

The superscript with the parentheses represents the order of the derivative

$$F^{(l)}(p) = \frac{d^l F}{dp^l}(p). \tag{9}$$

Roots of $\Lambda_k(\lambda)$ are eigenvalues of the linearized Vlasov equation around the reference stationary state F. Clearly, if there exists an eigenvalue whose real part is positive, then F is unstable. Due to (3), the destabilization of the profile F occurs through the first Fourier mode. Hence we use the first-order magnetization $M_1 > 0$ to quantify the instability, where

$$M_{1,x} + iM_{1,y} = M_1 e^{i\varphi_1} = \iint_\mu e^{iq} f(q, p) dq\, dp. \tag{10}$$

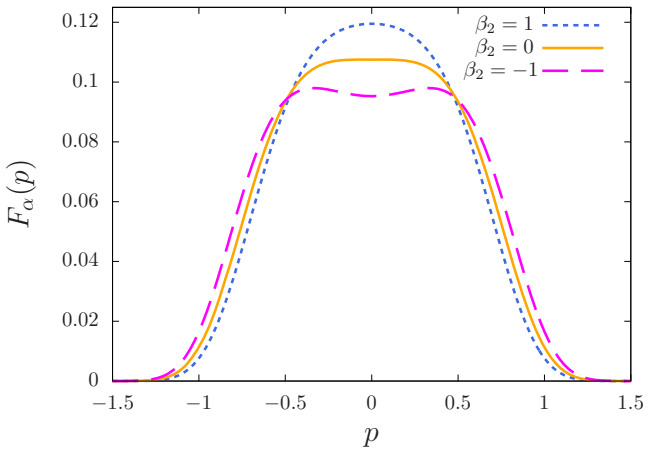

FIG. 2. Examples of the reference states $F_\alpha(p)$ (13) with $\beta_4 = 3$.

The second bifurcation parameter α is introduced as follows. We consider a family of homogeneous stationary states $\{F_\alpha(p)\}_\alpha$, which are even in p and such that $F_\alpha^{(2)}(0)$ changes sign at $\alpha = 0$. For simplicity, we take α so that

$$\alpha = F_\alpha^{(2)}(0). \tag{11}$$

We assume that $F_\alpha(p)$ is unimodal for $\alpha \leqslant 0$ and bimodal for $\alpha > 0$. The unimodality at $\alpha = 0$ implies that $F_0^{(4)}(0) < 0$ in general. Higher-order flatness, i.e., vanishing of higher-order derivatives at $p = 0$, will be discussed separately. There is a critical strength of the coupling constant K at which the reference state F_α changes stability. This critical point depends on α and is denoted by K_α^{c} (>0). We introduce the relative distance from the critical point as

$$\kappa_\alpha = \frac{K - K_\alpha^{\mathrm{c}}}{K_\alpha^{\mathrm{c}}}. \tag{12}$$

In the explicit computations of Secs. III and V, we use the family of stationary states

$$F_\alpha(p) = C \exp[-\beta_2 p^2/2 - (\beta_4 p^2/2)^2], \quad \beta_4 = 3, \tag{13}$$

where C is the normalization factor, so that F_α satisfies the normalization condition (5). The bifurcation parameter α is defined by

$$\alpha = F_\alpha^{(2)}(0) = -C\beta_2. \tag{14}$$

Some examples of $F_\alpha(p)$ are shown in Fig. 2.

III. LINEAR THEORY: EIGENVALUE COLLISION

The eigenvalue collision is derived from the linear theory of the Vlasov equation. The linearized Vlasov operator has a continuous spectrum spanning the whole imaginary axis. It may also have eigenvalues, given by the roots of the spectral functions (8). Since the instability occurs on the first Fourier mode [due to the condition (3)], the Λ_k functions for $k \neq \pm 1$ have no roots in the neighborhood of the bifurcation: Indeed, the existence of an eigenvalue λ would imply by Hamiltonian symmetry the existence of an eigenvalue $-\lambda$ and the reference state would be unstable. The spectral function Λ_{-1} satisfies the relation $\Lambda_{-1}(\lambda) = [\Lambda_1(\lambda^*)]^*$, where λ^* is the complex

conjugate of λ; hence we concentrate on

$$\Lambda_1(\lambda, \kappa_\alpha, \alpha) = 1 + (1+\kappa_\alpha) K_\alpha^{\rm c} \pi \int_{\mathbb{R}} \frac{F_\alpha^{(1)}(p)}{p - i\lambda} dp. \tag{15}$$

The model dependence appears solely in the coefficient K, i.e., κ_α in (15), so the linear theory is universal for all models satisfying (3).

We see from this expression that Λ_1 is holomorphic on the domains $\mathrm{Re}\,\lambda > 0$ and $\mathrm{Re}\,\lambda < 0$, but not on the whole complex plane. On the stable side of the bifurcation ($\kappa_\alpha < 0$), there are no eigenvalues; there are however Landau poles, which are roots of the analytically continued spectral function (15) from the right half plane $\mathrm{Re}\lambda > 0$ to the left half plane $\mathrm{Re}\lambda \leqslant 0$. The continuation is performed by continuously deforming the integration contour from $\mathbb{R}$ to a new contour L so as to avoid the singular point $p = i\lambda$, which is in the upper half of the complex p plane for $\mathrm{Re}\lambda > 0$, goes down on the real axis for $\mathrm{Re}\lambda = 0$, and moves to the lower half for $\mathrm{Re}\lambda < 0$ (see Appendix A 1 for more details). The continued integral is expressed for an analytic function $g(p)$ as

$$\int_L \frac{g(p)}{p - i\lambda} dp = \begin{cases} \int_{\mathbb{R}} \frac{g(p)}{p-i\lambda} dp & (\mathrm{Re}\lambda > 0) \\ \mathrm{P}\int_{\mathbb{R}} \frac{g(p)}{p-i\lambda} dp + i\pi g(i\lambda) & (\mathrm{Re}\lambda = 0) \\ \int_{\mathbb{R}} \frac{g(p)}{p-i\lambda} dp + i2\pi g(i\lambda) & (\mathrm{Re}\lambda < 0), \end{cases} \tag{16}$$

where the notation $\mathrm{P}\int \cdots$ stands for the Cauchy principal value. The second term in the second and third lines is the residue at $p = i\lambda$.

We approximately obtain an eigenvalue or a Landau pole λ by expanding the spectral function Λ_1 in a Taylor series of λ,

$$\Lambda_1(\lambda, \kappa_\alpha, \alpha) = -(1+\kappa_\alpha)(a_\alpha + b_\alpha \lambda - c_\alpha \lambda^2 + d_\alpha \lambda^3 + \cdots), \tag{17}$$

where

$$a_\alpha = \frac{\kappa_\alpha}{1+\kappa_\alpha} - \Lambda_1(0,0,\alpha), \quad b_\alpha = K_\alpha^{\rm c} \pi^2 \alpha,$$
$$c_\alpha = -\frac{1}{2} K_\alpha^{\rm c} \pi \int_{\mathbb{R}} \frac{F_\alpha^{(3)}(p)}{p} dp, \quad d_\alpha = -\frac{1}{3!} K_\alpha^{\rm c} \pi^2 F_\alpha^{(4)}(0). \tag{18}$$

Details of the above expansion are reported in Appendix A 1. We assume that $c_\alpha > 0$: This assumption implies that

$$\Lambda_1(0,0,\alpha) = 0 \quad (\alpha \leqslant 0),$$
$$\Lambda_1(0,0,\alpha) > 0 \quad (0 < \alpha < \alpha_1), \tag{19}$$

where $\alpha_1 > 0$ is a certain small value (see Appendix A 2). Since $\kappa_\alpha = 0$ corresponds to the critical line, we see from the first equation of (19) that for $\alpha \leqslant 0$ the critical eigenvalue crosses the imaginary axis at $\lambda = 0$ and the instability is nonoscillatory; from the second equation of (19) we see that for $\alpha > 0$ the critical eigenvalues cross the imaginary axis away from $\lambda = 0$ and the instability is oscillatory. The assumption $c_\alpha > 0$ is indeed true for the family (13) around $\alpha = 0$ (see Appendix A 3).

It is worth commenting that, from (17), (19), and the coefficient a_α, we have the relation

$$\Lambda_1(0, \kappa_\alpha, \alpha) = -\kappa_\alpha \quad (\alpha \leqslant 0). \tag{20}$$

For $\alpha > 0$ it is reasonable to assume that

$$\Lambda_1(0,0,\alpha) = O(\alpha) \quad (\alpha > 0). \tag{21}$$

We may also assume $d_\alpha > 0$ for sufficiently small $\alpha > 0$ since, from the unimodality hypothesis, $F_\alpha^{(4)}(0) < 0$ when $\alpha = 0$ and this inequality can be continued to small $|\alpha| > 0$.

Eigenvalues (or Landau poles) satisfy the equation

$$a_\alpha + b_\alpha \lambda - c_\alpha \lambda^2 + d_\alpha \lambda^3 + \cdots = 0. \tag{22}$$

We will use a truncated version of (22) to describe a sketch of the eigenvalue bifurcation diagram by computing eigenvalues or Landau poles at the eigenvalue collision point $\kappa_\alpha^{\rm col}$ and the critical point $\kappa_\alpha^{\rm c} = 0$; the order of truncation we use depends on the purpose.

The eigenvalue collision corresponds to the existence of a double root of Λ_1 and it can be captured by the quadratic equation

$$a_\alpha + b_\alpha \lambda - c_\alpha \lambda^2 = 0. \tag{23}$$

The degenerate real eigenvalue $\lambda_\alpha^{\rm col}$ is computed as

$$\lambda_\alpha^{\rm col} = \frac{b_\alpha}{2c_\alpha} < 0 \quad (\alpha < 0)$$
$$= 0 \quad (\alpha = 0)$$
$$> 0 \quad (\alpha > 0), \tag{24}$$

which is of $O(\alpha)$ due to $b_\alpha = O(\alpha)$. Substituting $\lambda_\alpha^{\rm col}$ into (23) and using (18), we have

$$\frac{\kappa_\alpha^{\rm col}}{1+\kappa_\alpha^{\rm col}} = \Lambda_1(0,0,\alpha) - \frac{b_\alpha^2}{4c_\alpha}. \tag{25}$$

Recalling (19) and the assumption $\Lambda_1(0,0,\alpha) = O(\alpha)$ for $\alpha > 0$, we have the following signs and scalings for the eigenvalue collision point $\kappa_\alpha^{\rm col}$:

$$\kappa_\alpha^{\rm col} < 0, \quad \kappa_\alpha^{\rm col} = O(\alpha^2) \quad (\alpha < 0),$$
$$\kappa_\alpha^{\rm col} = 0 \quad (\alpha = 0),$$
$$\kappa_\alpha^{\rm col} > 0, \quad \kappa_\alpha^{\rm col} = O(\alpha) \quad (\alpha > 0). \tag{26}$$

In order to estimate the purely imaginary critical eigenvalue $\lambda_\alpha^{\rm c} \in i\mathbb{R}$, which is embedded in the continuous spectrum, we truncate (22) at cubic order. Substituting $\lambda_\alpha^{\rm c} = iy$ ($y \in \mathbb{R}$) into

$$a_\alpha + b_\alpha \lambda - c_\alpha \lambda^2 + d_\alpha \lambda^3 = 0, \tag{27}$$

the imaginary part of (27) gives

$$\lambda_\alpha^{\rm c} = \begin{cases} 0 & (\alpha \leqslant 0) \\ \pm i\sqrt{\frac{b_\alpha}{d_\alpha}} & (\alpha > 0). \end{cases} \tag{28}$$

For the family (13), the eigenvalue collisions numerically computed from the continued spectrum function are shown in Fig. 3 with the α dependence of the critical point $K_\alpha^{\rm c}$. The sign of $\lambda_\alpha^{\rm col}$ (24) and the critical Landau pole (28) are confirmed. The scalings (26) will be confirmed in Sec. V after discussing the trapping scaling and the jump in the nonlinearly saturated amplitude in Sec. IV.

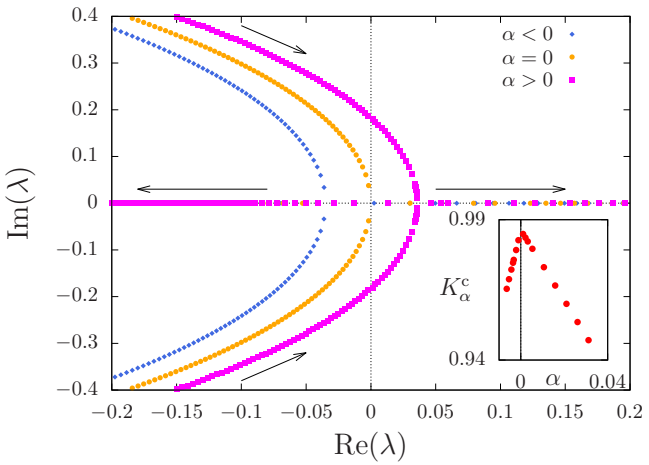

FIG. 3. Collisions of eigenvalues and Landau poles for the family (13) close to the codimension-two bifurcation point. Here $\beta_2 = 0.3$ (unimodal $\alpha < 0$, blue diamonds), $\beta_2 = 0$ (flat $\alpha = 0$, orange circles), and $\beta_2 = -0.3$ (bimodal $\alpha > 0$, magenta squares) from left to right. The arrows indicate the movement of eigenvalues and Landau poles as K increases. The inset shows the critical point K_α^c as a function of α; we note an apparent singular maximum of this function at $\alpha = 0$.

IV. NONLINEAR THEORY: TRAPPING SCALING AND JUMP

After the reference state becomes unstable, the system reaches an asymptotic state which is close to the reference state: The bifurcation is continuous, except for $\alpha = 0$. This is the region where the trapping scaling $A_{\rm sat} = O((\mathrm{Re}\lambda)^2)$ is valid. When the parameter controlling the instability is further increased, a jump in $A_{\rm sat}$ follows the continuous bifurcation. To understand these features, we apply a nonlinear theory, the self-consistent equation, which is a powerful tool for Vlasov and Vlasov-like equations. We sketch the derivation of the self-consistent equations in Sec. IV A; in Sec. IV B, we expand them into (half-integer) power series of the magnetizations and explain why considering only the dominant magnetization M_1 in the HMF model is sufficient to ensure universality of the bifurcation diagram, as for the linear computation. Using this expansion, we discuss the continuity of the bifurcation in Sec. IV C. For $\alpha < 0$ (unimodal), we show in Sec. IV D that the well-known trapping scaling $O((\mathrm{Re}\lambda)^2)$ is reproduced by the self-consistent equation and that the scaling of the jump point $\kappa_\alpha^{\rm J} = O(|\alpha|^{3/2})$ is also predicted. The self-consistent equation has a limitation: The asymptotic state must be stationary; this condition is not satisfied for small $\alpha > 0$ (bimodal). We therefore propose another theory to predict the scaling: $\kappa_\alpha^{\rm J} = O(\alpha)$ for $\alpha > 0$ in Sec. IV E. The investigation of the trapping scaling for $\alpha > 0$ is left for numerical examinations.

A. Self-consistent equation

The idea of the self-consistent equation is to assume that there exists an asymptotic stationary state $F_\alpha^{\rm asym}$ and make the approximation that the temporal evolution is governed by the Hamiltonian corresponding to this asymptotic state $H_\alpha^{\rm asym} = H[F_\alpha^{\rm asym}]$. Introducing the kth magnetizations in the asymptotic state

$$M_{k,x} + iM_{k,y} = \iint_\mu e^{ikq} F_\alpha^{\rm asym}(q,p)dq\,dp, \tag{29}$$

the asymptotic Hamiltonian is

$$H_\alpha^{\rm asym} = \frac{p^2}{2} - \sum_{k=1}^{\infty} K_k[M_{k,x}\cos(kq) + M_{k,y}\sin(kq)]. \tag{30}$$

The asymptotic Hamiltonian system is integrable, so we can introduce angle-action variables (θ, J). The temporal dynamics driven by $H_\alpha^{\rm asym}$ conserves the action and evolves linearly the angle. The asymptotic state is then obtained by taking the average of the initial reference state $F_\alpha(p)$ over the θ variable, at fixed J,

$$F_\alpha^{\rm asym}(J) = \frac{1}{2\pi}\int_0^{2\pi} F_\alpha(p(\theta,J))d\theta =: \langle F_\alpha\rangle_J, \tag{31}$$

where the symbol $\langle\cdot\rangle_J$ represents the average over θ on a fixed-J contour. The right-hand side $\langle F_\alpha\rangle_J$ actually depends on the asymptotic state, in other words, on $\boldsymbol{M} = (M_1, M_2, \ldots)$, through the definition of angle-action variables; hence Eq. (31) must be solved self-consistently. We assume $M_{k,y} = 0$ and $M_{k,x} > 0$ and define $M_k = M_{k,x}$. The self-consistent equations are

$$M_k = \iint_\mu \cos(kq)\langle F_\alpha\rangle_J dq\,dp \quad (k = 1, 2, \ldots). \tag{32}$$

We start with three remarks. First, we have to assume the existence of an asymptotic stationary state. The bimodal case with small $\alpha > 0$ is then out of scope, since the two peaks in the velocity profile induce two resonances and the two resonances create two traveling clusters at opposite velocities. This two-cluster state is not stationary. Second, although the self-consistent equation is only approximate, it has been already proved to be powerful to analyze the critical behavior, when $|F_\alpha^{\rm asym} - F_\alpha|$ is sufficiently small around the critical point [34]. Third, the asymptotic state (31) conserves all Casimir invariants up to linear order in $F_\alpha^{\rm asym} - F_\alpha$, that is,

$$\mathcal{C}\big[F_\alpha^{\rm asym}\big] - \mathcal{C}[F_\alpha] = O\big(\big|F_\alpha^{\rm asym} - F_\alpha\big|^2\big). \tag{33}$$

B. Expansion of the self-consistent equations

Expanding the self-consistent equation (32) into a power series of $\boldsymbol{M}$ and picking up the leading two terms, we estimate $M_k = O(\alpha M_1^{3/2})$ $(k > 1)$ (see in Appendix B 1). This scaling suggests that for small $|\alpha|$, the higher-order $k > 1$ magnetizations have a negligible effect and the analysis of the HMF model should be valid for any interaction potential ϕ.

We denote from now on M_1 by M for simplicity. In the HMF model, the expanded self-consistent equation is [23]

$$\Lambda_1(0, \kappa_\alpha, \alpha)M = \varphi(M)M, \tag{34}$$

where

$$\varphi(M) := L_{3/2}M^{1/2} + L_{5/2}M^{3/2} + L_3M^2 + \cdots. \tag{35}$$

The coefficients $L_{3/2}$ and $L_{5/2}$ are proportional to derivatives of F_α:

$$L_{3/2} = \tilde{L}_{3/2} F_\alpha^{(2)}(0) = \tilde{L}_{3/2}\alpha,$$
$$L_{5/2} = \tilde{L}_{5/2} F_\alpha^{(4)}(0). \tag{36}$$

The one-particle dynamics in the HMF model is essentially a pendulum and the angle-action variables (θ, J) have explicit expressions in terms of Legendre elliptic functions and integrals (see [35], for instance). Using the expressions, we have

$$\tilde{L}_{3/2} \simeq 5.168, \quad \tilde{L}_{5/2} \simeq -0.089. \tag{37}$$

The exact values above as well as the vanishing $O(M)$ term in $\varphi(M)$ are specific to the HMF model, but the signs and smallness of the $O(M)$ term hold around the codimension-two bifurcation point for a generic system, i.e., a generic coupling function ϕ. We thus analyze the continuity of the bifurcation using (34).

C. Continuity of the bifurcation

Solutions to the self-consistent equation (34) are obtained as intersection points of the graph of $\varphi(M)$ with the horizontal level $\Lambda_1(0, \kappa_\alpha, \alpha)$, which is a decreasing function of κ_α around $\alpha = 0$. To graphically understand the intersection, we consider a scaled and truncated function $\varphi_{\rm scale}(M)$ defined by

$$\varphi_{\rm scale}(M) = rM^{1/2} + M^{3/2} - \gamma M^2, \tag{38}$$

which is obtained by scaling (35) as

$$\sqrt{M} \to \frac{-\gamma L_{5/2}}{L_3}\sqrt{M}, \quad \varphi \to \frac{-\gamma^3 L_{5/2}^4}{L_3^3}\varphi, \quad r = \frac{L_3^2 L_{3/2}}{\gamma^2 L_{5/2}^3}. \tag{39}$$

Here we use the sign $L_{5/2} > 0$ from $F_0^{(4)}(0) < 0$ and continuation around $\alpha = 0$. Moreover, we assume that $L_3 < 0$ and $\gamma > 0$ because it is the case for $F_0(p)$ in the HMF model (see Appendix B 2). The sign of r coincides with the sign of α. Graphs of $\varphi_{\rm scale}(M)$ are shown in Fig. 4 for $\gamma = 1.2$. An increasing interval of $\varphi_{\rm scale}(M)$ corresponds to an unstable branch, because M at the intersection point decreases when κ_α increases.

For $\alpha < 0$, a stable branch exists around $M = 0$ and the bifurcation is continuous. Further increasing κ_α, the stable branch vanishes and a jump emerges, when the level $\Lambda_1(0, \kappa_\alpha, \alpha)$ is lower than $\varphi_{\rm min}$, which is the local minimum of $\varphi(M)$ located around $M = 0$ [see Fig. 4(b)]. For $\alpha \geqslant 0$, there is no stable branch around $M = 0$: The self-consistent equation predicts that the bifurcation is discontinuous. The discontinuity for $\alpha = 0$ is also predicted by the unstable manifold expansion, reported in Appendix C. The discontinuity disagrees for $\alpha > 0$ with Fig. 1 and with the numerical simulations. There is no contradiction however: As already commented above and as we will see in the simulations, the asymptotic state for $\alpha > 0$ and very close to criticality is not stationary and is then out of the scope of the self-consistent equation.

We note that smallness of $|\alpha|$ is crucial to have the local minimum $\varphi_{\rm min}$ for $\alpha < 0$. Indeed, as shown in Fig. 5, the local minimum disappears if $|r|$ is sufficiently large. Recalling $r = O(\alpha)$, we conclude that the jump following a continuous

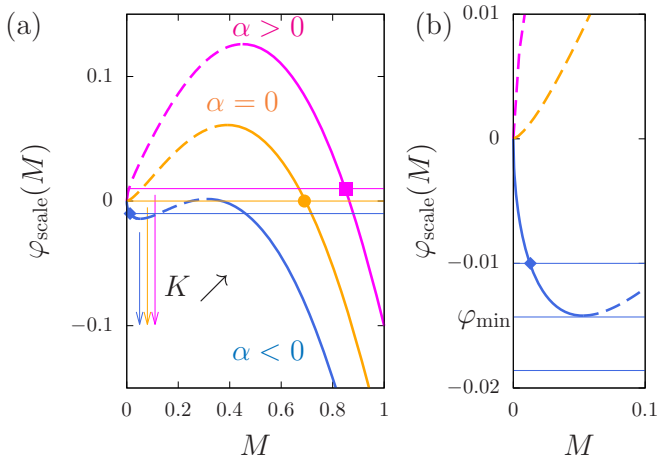

FIG. 4. (a) Schematic picture of $\varphi_{\rm scale}(M)$ (38) for $r = -0.1$ ($\alpha < 0$, blue lower curve), $r = 0$ ($\alpha = 0$, orange middle curve), and $r = 0.1$ ($\alpha > 0$ magenta upper curve) with $\gamma = 1.2$. A solid line represents a stable branch and a dashed line an unstable branch. The three horizontal lines mark the level of $\Lambda_1(0, \kappa_\alpha, \alpha)$, which goes down as the coupling constant K increases from the critical value $K_\alpha^{\rm c}$. The three points predict the asymptotic value of M for $\alpha < 0$ and $\kappa_\alpha > 0$ (blue diamond), $\alpha = 0$ and $\kappa_\alpha = 0^+$ (orange circle), and $\alpha > 0$ and $\kappa_\alpha = 0^+$ (magenta square). Actually, this jump of M does not happen for $\alpha > 0$ (see the text). (b) Magnification of (a) around the origin. The middle of the three horizontal blue lines is the jump level at $K_\alpha^{\rm J}$, determined from $\varphi_{\rm min}$ by (44), and M jumps to the other stable branch of (a) for $K > K_\alpha^{\rm J}$.

bifurcation is produced by flatness of $F_\alpha(p)$ around $p = 0$ in $\alpha < 0$ (unimodal) and disappears for large $|\alpha|$. This dependence on α is consistent with Fig. 15 of Ref. [7].

We further remark that the discontinuity for $\alpha = 0$ actually carries over for higher-order flatness of $F_0(p)$: Any $F_0(p)$ with a nonconstant leading term of $O(p^{2n})$ ($n \geqslant 3$) makes the bifurcation discontinuous, as discussed in Appendix D. An extreme case is the water-bag distribution, which is perfectly flat around $p = 0$ and which is known to induce a

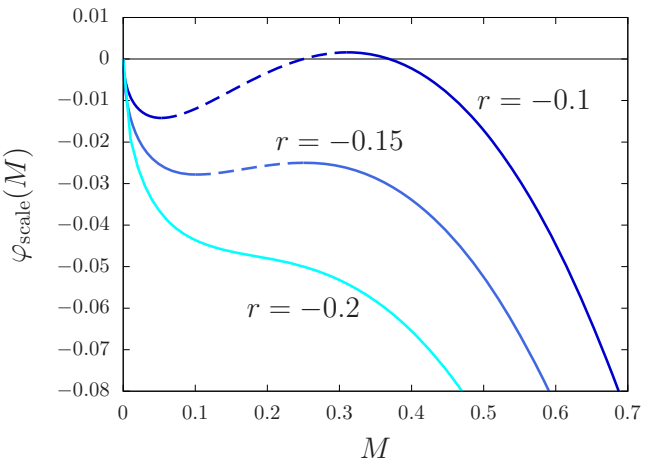

FIG. 5. Graphs of $\varphi_{\rm scale}(M)$ (38) with $\gamma = 1.2$. A solid part is a stable branch and a dashed part is an unstable branch. The unstable branch and a jump disappear when $|r|$ is sufficiently large.

discontinuous bifurcation [12]. The above result implies that $n = 2$ is sufficiently flat to make the bifurcation discontinuous.

D. Trapping scaling and jump location for $\alpha \leqslant 0$

The trapping scaling $M = O((\mathrm{Re}\lambda)^2)$ is well known and is reproduced by the self-consistent equation. First, we observe the linear relation

$$\kappa_\alpha = O(\mathrm{Re}\lambda) \tag{40}$$

from the eigenvalue problem up to the linear term

$$a_\alpha + b_\alpha \lambda = 0, \tag{41}$$

where $a_\alpha = \kappa_\alpha/(1+\kappa_\alpha)$ for $\alpha \leqslant 0$. Second, the self-consistent equation up to the leading term of $\varphi(M)$ is

$$\Lambda_1(0, \kappa_\alpha, \alpha) = L_{3/2} M^{1/2} \tag{42}$$

for $M > 0$. The trapping scaling then results from relations (20) and (36):

$$M = \left(\frac{\kappa_\alpha}{-L_{3/2}}\right)^2 = O((\mathrm{Re}\lambda)^2/\alpha^2). \tag{43}$$

This dependence on α suggests a discontinuity at $\alpha = 0$.

We compute now the α dependence of the jump point $\kappa_\alpha^{\mathrm{J}}$. The self-consistent equation has a nonzero stable solution around $M = 0$ if $\Lambda_1(0, \kappa_\alpha, \alpha) \geqslant \varphi_{\min}$ and loses this stable solution if $\Lambda_1(0, \kappa_\alpha, \alpha) < \varphi_{\min}$. The jump point $\kappa_\alpha^{\mathrm{J}}$ is hence computed by the equation

$$\Lambda_1\left(0, \kappa_\alpha^{\mathrm{J}}, \alpha\right) = \varphi_{\min}, \tag{44}$$

where, using the expansion of φ up to $O(M^{3/2})$,

$$\varphi_{\min} = -\frac{2}{3}\frac{(-L_{3/2})^{3/2}}{(3L_{5/2})^{1/2}}. \tag{45}$$

The relations (20) and (36) then provide the scaling

$$\kappa_\alpha^{\mathrm{J}} = \frac{2}{3}\frac{(-L_{3/2})^{3/2}}{(3L_{5/2})^{1/2}} = O(|\alpha|^{3/2}) \quad (\alpha \leqslant 0). \tag{46}$$

The prefactor of $|\alpha|^{3/2}$ is given in Appendix E.

E. Scaling of the jump location for $\alpha > 0$

Since the self-consistent equation is *a priori* not valid in this case, we propose a heuristic mechanism to explain the continuous bifurcation and the jump in the bimodal case (drawing ideas from [36]). Let λ be an eigenvalue. The two peaks of $F_\alpha(p)$ create two traveling clusters around the momentum $p = \pm\mathrm{Im}\lambda$ and the system may be trapped in such a nonstationary bicluster asymptotic state. The width of the clusters is of $O(\sqrt{M})$, which is expected to be of $O(\mathrm{Re}\lambda)$ from the trapping scaling $M = O((\mathrm{Re}\lambda)^2)$ (this will be checked in Sec. V). This nonstationary asymptotic state is expected to disappear when the two clusters start to overlap, because this will trigger their merging; this happens when $\mathrm{Im}\lambda \simeq O(\mathrm{Re}\lambda)$. After merging, a single cluster forms and the system goes to a stationary state which is predicted by the self-consistent equation: This is the jump.

The critical eigenvalue $\lambda_\alpha^{\mathrm{c}}$ and the eigenvalue at the eigenvalue collision point $\lambda_\alpha^{\mathrm{col}}$, corresponding, by definition, to $\kappa_\alpha^c = 0$ and $\kappa_\alpha^{\mathrm{col}} > 0$, respectively, satisfy

$$\begin{aligned} \mathrm{Re}\lambda_\alpha^{\mathrm{c}} &= 0, \qquad \mathrm{Im}\lambda_\alpha^{\mathrm{c}} = O(\sqrt{\alpha}), \\ \mathrm{Re}\lambda_\alpha^{\mathrm{col}} &= O(\alpha), \quad \mathrm{Im}\lambda_\alpha^{\mathrm{col}} = 0. \end{aligned} \tag{47}$$

We also know that $\mathrm{Im}\lambda$ ($\mathrm{Re}\lambda$) is a decreasing (increasing) function of κ_α [see Fig. 3(c)] and $\kappa_\alpha^{\mathrm{col}} = O(\alpha)$.

Clearly, the cluster merging condition $\mathrm{Im}\lambda \simeq \mathrm{Re}\lambda$ is reached for $\kappa_\alpha^{\mathrm{J}}$ somewhere in the interval $0 = \kappa_\alpha^{\mathrm{c}} < \kappa_\alpha^{\mathrm{J}} < \kappa_\alpha^{\mathrm{col}} = O(\alpha)$. Hence $\kappa_\alpha^{\mathrm{J}}$ is at most of order α. Furthermore, if $\kappa_\alpha \ll \alpha$, then

$$\mathrm{Re}\lambda_\alpha = O(\alpha), \quad \mathrm{Im}\lambda_\alpha = O(\sqrt{\alpha}),$$

so the merging condition $\mathrm{Im}\lambda \simeq \mathrm{Re}\lambda$ can never be met. We conclude that

$$\kappa_\alpha^{\mathrm{J}} = O(\alpha) \quad (\alpha > 0), \tag{48}$$

consistently with Fig. 1.

V. NUMERICS

We now illustrate and complement with detailed numerical simulations the results of previous sections.

A. Simulation setup

We use the coupling function

$$\phi(q) = -[K\cos(q) + K_2\cos(2q)],$$

where $K_2 = 0.5$ is fixed and K is used as a bifurcation parameter. We remark that K_2 is smaller than the critical point K_α^{c} reported in the inset of Fig. 3. The reference family is (13) and

$$\alpha = F_\alpha^{(2)}(0) = -C\beta_2 \tag{49}$$

is the second bifurcation parameter. The initial condition is prepared as

$$F(q, p, t = 0) = F_\alpha(p)(1 + \epsilon\cos q) \tag{50}$$

and the strength of perturbation is fixed as $\epsilon = 10^{-6}$.

We perform numerical simulations of the Vlasov equation by the semi-Lagrangian method described in [37] with the time step $\Delta t = 0.05$. The phase space (q, p) is truncated as $(-\pi, \pi] \times [-4, 4]$, where the maximum value $|p| = 4$ is large enough (see Fig. 2). We divide the phase space into an $L \times L$ mesh and we fix $L = 512$ in the following computations. We have checked that $L = 1024$ does not significantly modify the results for $\beta_2 = 0.03$ and 0.05.

B. Scaling relation between $\mathrm{Re}\lambda$ and $K - K_\alpha^{\mathrm{c}}$

The instability rate $\mathrm{Re}\lambda$ is commonly used as a bifurcation parameter; for instance, the universal trapping scaling is usually expressed as $M = O((\mathrm{Re}\lambda)^2)$ on the unstable side around the critical point. However, we will typically show curves of the magnetization as a function of the coupling constant K or κ_α.

In principle, the choice between $\mathrm{Re}\lambda$ and κ_α is arbitrary, as there is a linear relation between them (40); however, for α

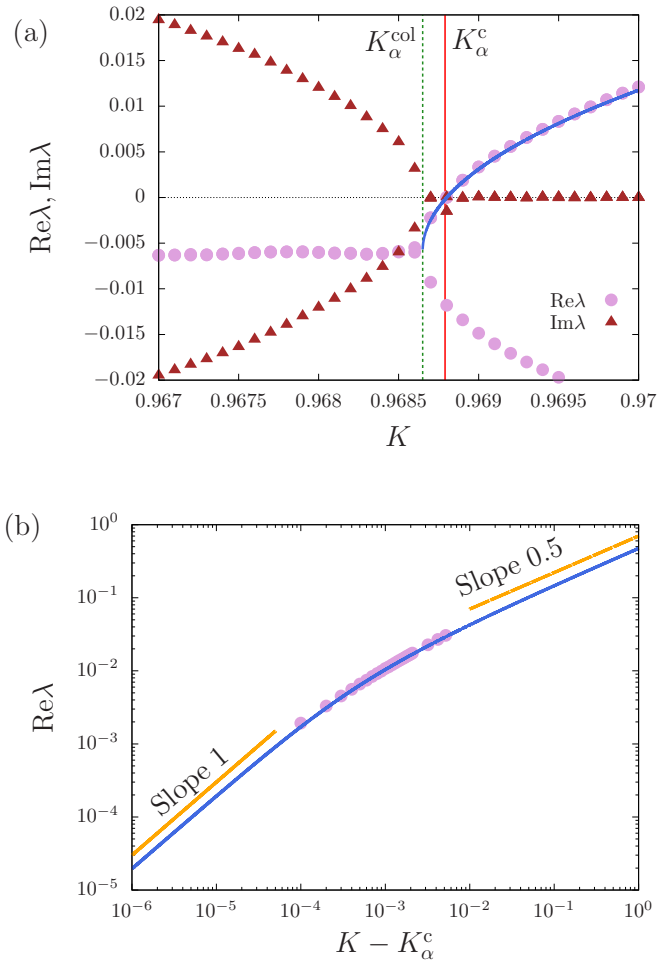

FIG. 6. (a) Bifurcation of Landau poles, with $\alpha = -0.0054$ ($\beta_2 = 0.05$). Here Reλ (plum circles) and Imλ (brown triangles) are plotted as functions of K. The blue solid curve represents the curve (51). The green dotted and red solid vertical lines mark the eigenvalue collision point $K_\alpha^{\rm col}$ and the critical point $K_\alpha^{\rm c}$, respectively. (b) Instability Reλ as a function of $K - K_\alpha^{\rm c}$ in logarithmic scale. The blue solid curve represents the curve (51).

close to 0, this linear relation is restricted to a narrow interval of κ_α around 0. For $\alpha > 0$ ($\beta_2 < 0$), the narrowness of the region is clear, since the linear relation between Reλ and κ_α does not hold after the eigenvalue collision $\kappa_\alpha > \kappa_\alpha^{\rm col}$ and the eigenvalue collision point $\kappa_\alpha^{\rm col}$ approaches the critical point $\kappa_\alpha^{\rm c} = 0$ as α goes to 0. For $\alpha < 0$ ($\beta_2 > 0$), the narrowness of the linear region is illustrated in Fig. 6. Figure 6(a) reports the bifurcation diagram of Landau poles for $\beta_2 = 0.05$, which corresponds to $\alpha = -0.0054$. The unstable branch of Reλ is approximated by

$$\mathrm{Re}\lambda = 0.48\left(\sqrt{K - K_\alpha^{\rm col}} - \sqrt{K_\alpha^{\rm c} - K_\alpha^{\rm col}}\right), \tag{51}$$

where

$$K_\alpha^{\rm c} \simeq 0.968\,79, \quad K_\alpha^{\rm col} \simeq 0.968\,65. \tag{52}$$

Due to the smallness of $K_\alpha^{\rm c} - K_\alpha^{\rm col} \simeq 1.4 \times 10^{-4}$, the linear region is restricted to $K - K_\alpha^{\rm c} < 10^{-4}$, as shown in Fig. 6(b). Working in this region is very demanding numerically. Therefore, we will test the trapping scaling and the jump scaling by observing M as a function of $K - K_\alpha^{\rm c}$ or κ_α rather than of Reλ.

C. Scaling region and jump

We use three estimators for the amplitude of the magnetization in the saturated state: the average

$$M_{\rm ave} = \frac{2}{T}\int_{T/2}^{T} M(t)dt, \tag{53}$$

the maximum

$$M_{\rm max} = \max_{t\in[0,T]} M(t), \tag{54}$$

and the first peak height $M_{\rm fp}$ of $M(t)$. The upper limit of time is set as $T = 3000$. These estimators are shown in Fig. 7 as functions of K. As the theory predicted, we find a jump in each panel. The orders of magnitude of the collision point $K_\alpha^{\rm col}$, the critical point $K_\alpha^{\rm c}$, and the jump point $K_\alpha^{\rm J}$ perfectly agree with Fig. 1. The trapping scaling $M = O(\kappa_\alpha^2)$ is also confirmed in the insets of Figs. 7(a) and 7(c).

The existence of a jump is directly confirmed from the temporal evolution of $M(t)$, which is reported in Fig. 8 around the jump point $K_\alpha^{\rm J}$. Note that in Fig. 8(b) $M(t)$ is very small for $K = 0.9863 > K_\alpha^{\rm J}$, but this is caused by the slow dynamics around the critical point. Indeed, $M(t)$ tends to slowly increase. We remark that the slow dynamics induces a small gap between the critical point $K_\alpha^{\rm c}$ and the jump point $K_\alpha^{\rm J}$ in Fig. 7(b).

A numerically obtained bifurcation diagram is reported in Fig. 9(a), which is quantitatively in good agreement with Fig. 1(a). For $\alpha > 0$, Fig. 9(a) verifies the linear scaling of the eigenvalue collision $\kappa_\alpha^{\rm col} = O(\alpha)$ (26) and of the jump $\kappa_\alpha^{\rm J} = O(\alpha)$ (see Sec. IV E). For $\alpha < 0$, Figs. 9(b) and 9(c) confirm the collision scaling $\kappa_\alpha^{\rm col} = 5.34\alpha^2$ (26) and the jump point scaling $\kappa_\alpha^{\rm J} = 6.29|\alpha|^{3/2}$ (46), respectively, although the theoretical prefactor 6.29 is somewhat larger than the numerically obtained value 4.71 (a similar effect is seen in [23]). See Appendix E for the computation of theoretical prefactors for $\alpha \leqslant 0$.

We assess the universality of the bifurcation diagram through the scaling of M_2, which is theoretically predicted in Appendix B 1 to be $M_2 = O(\alpha M_1^{3/2})$, namely, $M_2 = O(\alpha\kappa_\alpha^3)$, for a fixed $\alpha < 0$ (unimodal). This scaling with respect to κ_α is verified in Fig. 10. Beyond the scaling with κ_α, the magnitude of M_2 also suggests the validity of the scaling factor α, since M_2 is much smaller than $M_1^{3/2}$ in the scaling region. Therefore, we conclude that the theory is valid and for small $|\alpha|$ the higher-order magnetizations M_k ($k > 1$) are negligible for a general interaction potential ϕ in (1) and (2).

D. Existence of two traveling clusters

Finally, we examine the existence of two traveling clusters for $\alpha > 0$ in the interval between $K_\alpha^{\rm c}$ and $K_\alpha^{\rm J}$. These clusters are very small and cannot be observed directly on the phase space density. Instead we observe the angular frequency ω of $M(t)$, which is extracted as the peak position of the power spectrum density. A complex eigenvalue λ induces an oscillation with angular frequency Imλ, but the existence of the two traveling clusters at $p = \pm\mathrm{Im}\lambda$ induces the double angular

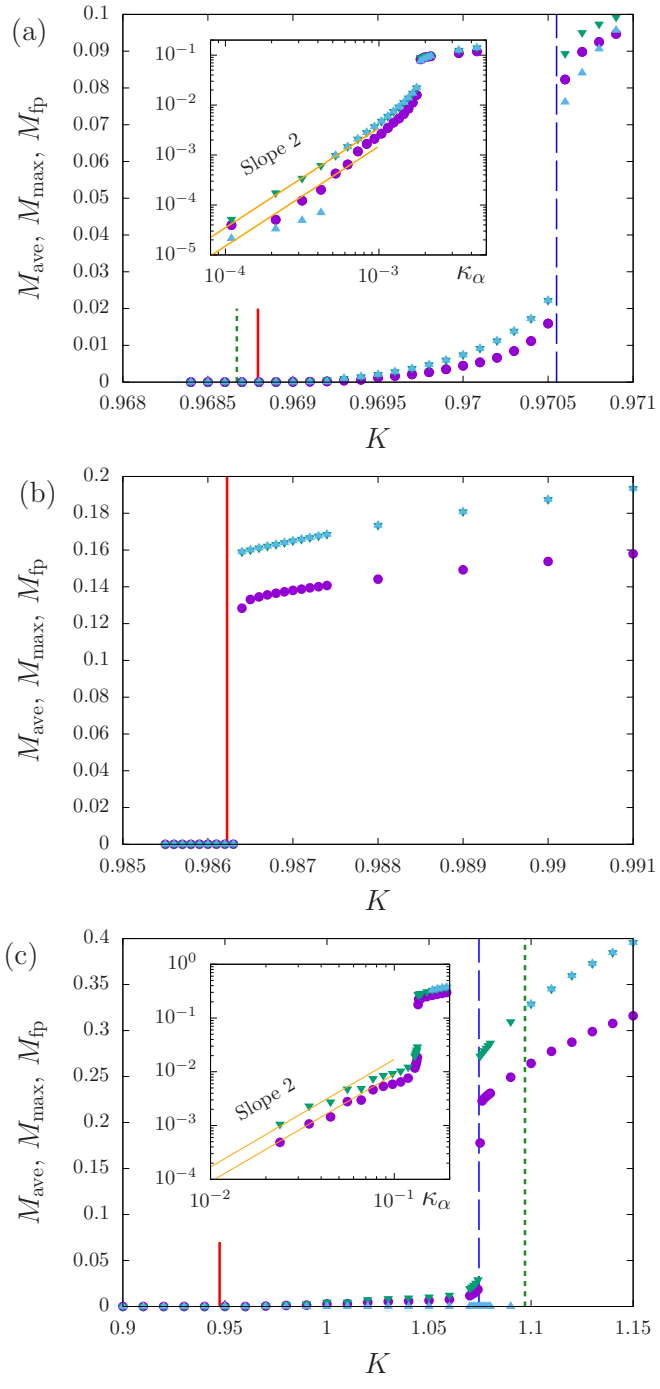

FIG. 7. Plots of $M_{\rm ave}$ (purple circles), $M_{\rm max}$ (green inverse triangles), and $M_{\rm fp}$ (blue triangles) as functions of K, with (a) $\beta_2 = 0.05$ (unimodal $\alpha < 0$), (b) $\beta_2 = 0$ (flat $\alpha = 0$), and (c) $\beta_2 = -0.3$ (bimodal $\alpha > 0$). In all panels, the red solid, green dotted, and blue dashed vertical lines represent the critical point $K_\alpha^{\rm c}$, the eigenvalue collision point $K_\alpha^{\rm col}$ (computed from the linear theory), and the jump point $K_\alpha^{\rm J}$ (estimated from the numerics); the three lines coincide in (b). In (a) and (c) the insets show the three estimators against κ_α in logarithmic scale. The orange straight lines have slope 2 (consistent with trapping scaling) and are guides for the eyes.

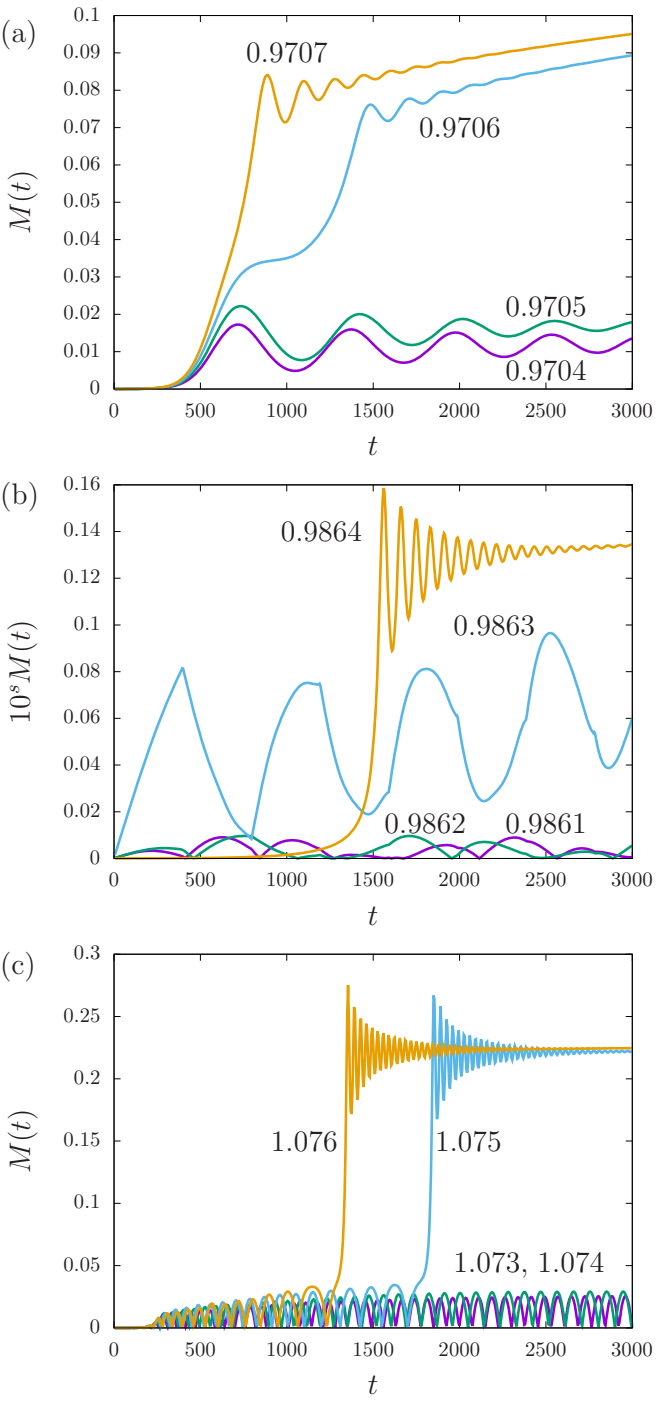

FIG. 8. Temporal evolution of $M(t)$ around the jump point $K_\alpha^{\rm J}$, with (a) $\beta_2 = 0.05$ (unimodal $\alpha < 0$), (b) $\beta_2 = 0$ (flat $\alpha = 0$), and (c) $\beta_2 = -0.3$ (bimodal $\alpha > 0$). The numbers in the panels represent the value of K. The magnetization $M(t)$ is scaled to $10^s M(t)$ in (b); $s = 2$ for $K = 0.9861$ and 0.9862, $s = 3$ for $K = 0.9863$, and $s = 0$ for $K = 0.9864$.

frequency $\omega = 2\,{\rm Im}\lambda$. Indeed, this relation is confirmed in Fig. 11, which supports the existence of the two traveling clusters.

VI. CONCLUSION

We have investigated in detail the bifurcation occurring in a Vlasov equation when a family of stationary states with a small curvature at the critical velocity (taken to be 0 in this article) becomes unstable. Our main result is that the

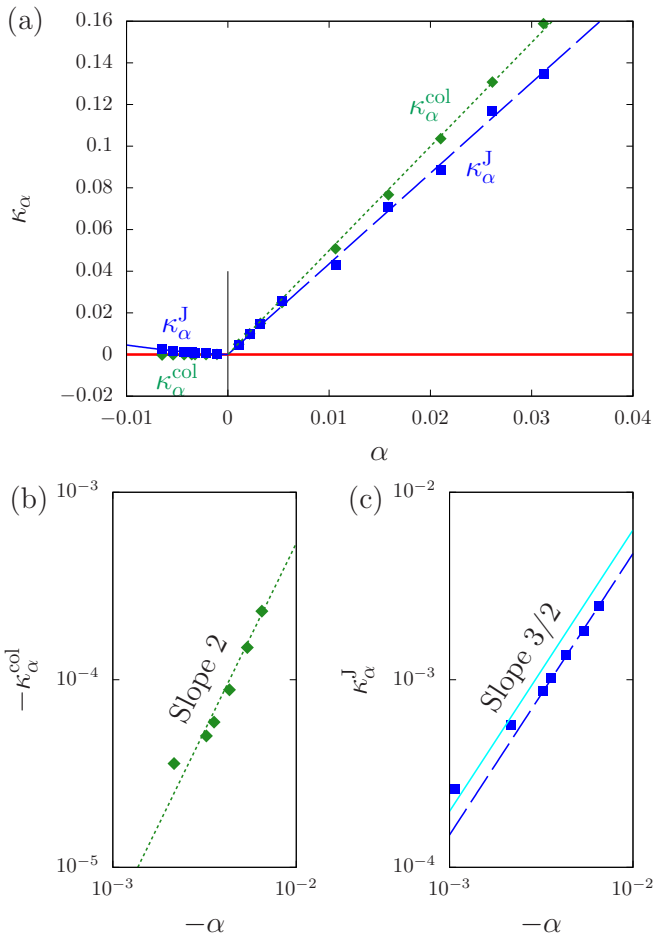

FIG. 9. (a) Numerically obtained bifurcation diagram on the plane (α, κ_α), which corresponds to Fig. 1(a). The red solid line is the critical line. The green diamonds show the eigenvalue collision point $\kappa_\alpha^{\rm col}$ and the blue squares the jump point $\kappa_\alpha^{\rm J}$. (b) Scaling of the eigenvalue collision for $\alpha < 0$ with the theoretical line $-\kappa_\alpha^{\rm col} = 5.34\alpha^2$ (green dotted). (c) Scaling of the jump for $\alpha < 0$ with the theoretical line $\kappa_\alpha^{\rm J} = 6.29|\alpha|^{3/2}$ (light blue solid) and the estimated line with the prefactor 4.71 (blue dashed).

codimension-two bifurcation point where the curvature is zero corresponds to a collision of generalized eigenvalues happening precisely at the stability boundary. At this point the magnetization is discontinuous and away from this point and on both sides the bifurcation is continuous and followed by a jump. Due to this jump, the region where trapping scaling can be observed shrinks on both sides of the codimension-two bifurcation point. Our theoretical analyses based on the self-consistent equation qualitatively predict this phenomenology around the codimension-two bifurcation point and the predictions are fully confirmed by direct numerical simulations.

Although the analysis and numerical simulations were performed in the simplified context of a periodic one-dimensional Vlasov equation with attractive potential, we certainly expect that the uncovered bifurcation is generic and could be found in physical systems sharing the same qualitative properties. The two-dimensional Euler equation shares many properties with the Vlasov equation; hence we expect the bifurcation described in this article can be found, for instance, for vortices in two-dimensional fluids, which can also model electron beams [38,39], or for other shear flows [10,40]. Self-organizing atoms in optical cavities could also provide an experimental test bed [41], but would require one to understand the role of a small dissipation (see [42] for shear flows).

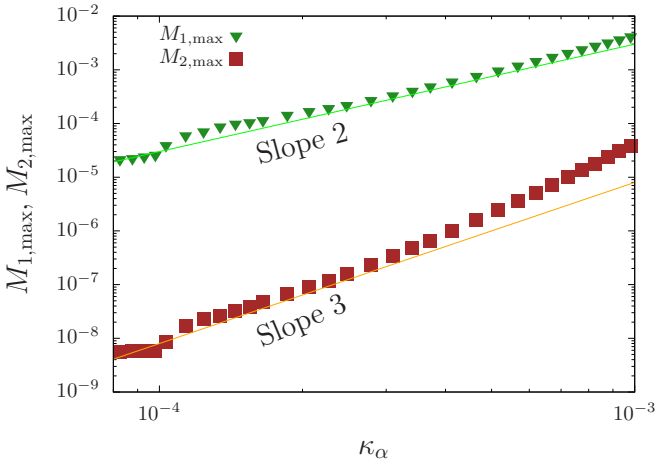

FIG. 10. Scalings of $M_{1,\max} = O(\kappa_\alpha^2)$ and $M_{2,\max} = O(\kappa_\alpha^3)$, where $M_{k,\max} = \max_{t\in[0,3000]} M_k(t)$ $(k = 1, 2)$ and $M_{1,\max} = M_{\max}$, with $\beta_2 = 0.05$ (unimodal $\alpha = -0.0054$), which gives $K_\alpha^{\rm c} \simeq 0.968\,794$. The magnitude of $M_{2,\max}$ suggests the validity of the scaling factor α in the predicted relation $M_2 = O(\alpha M_1^{3/2})$. More precise computations are needed for $\kappa_\alpha < 10^{-4}$.

On the theoretical side, these results are a further step towards a classification of bifurcations in Vlasov systems [15]. Several questions remain open however. The self-consistent equation approach is restricted to the unimodal side of the bifurcation; hence our description of the bimodal side is mainly numerical. Even on the unimodal side, a better theory would

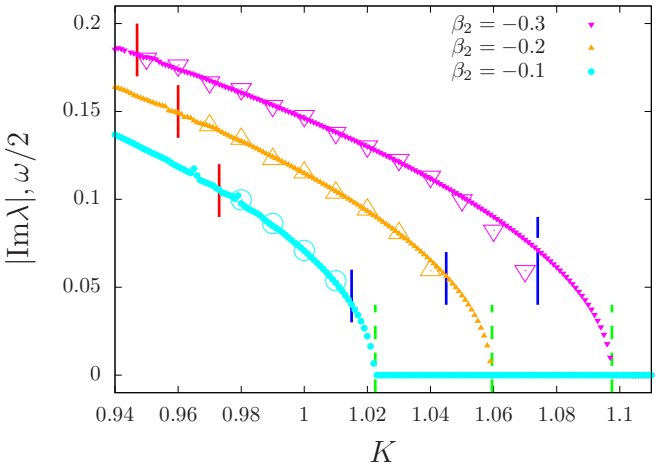

FIG. 11. Comparison between $|{\rm Im}\lambda|$ (small symbols) and $\omega/2$ (large symbols), where ω is estimated from a time series of $M(t)$, with $\alpha = -C\beta_2 > 0$ and $\beta_2 = -0.1$ (light blue circles), -0.2 (orange triangles), and -0.3 (magenta inverted triangles). Red, blue, and green vertical segments mark the critical point $K_\alpha^{\rm c}$, the jump point $K_\alpha^{\rm J}$ (estimated from the numerics), and the collision point $K_\alpha^{\rm col}$, respectively.

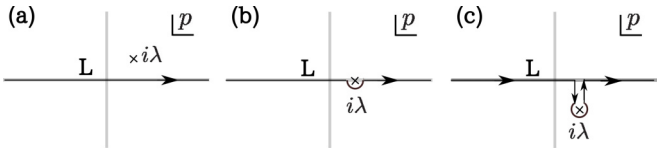

FIG. 12. The integration contour (black line) is $L = \mathbb{R}$ for (a) $\mathrm{Re}\lambda > 0$; it includes (b) a half circle for $\mathrm{Re}\lambda = 0$ and (c) a full circle for $\mathrm{Re}\lambda < 0$.

be welcome; it would entail a real description of the phase space and possibly a generalization of the single-wave model. This is probably challenging.

ACKNOWLEDGMENTS

Y.Y.Y. acknowledges support from JSPS KAKENHI Grants No. JP16K05472 and No. JP21K03402. This work was supported by the projects RETENU, Project No. ANR-20-CE40-0005-01, and PERISTOCH, Project No. ANR-19-CE40-0023, of the French National Research Agency.

APPENDIX A: LINEAR ANALYSIS

1. Expansion of the spectrum function

We first recall how the spectrum function is defined for any $\lambda \in \mathbb{C}$ by analytical continuation. For $\mathrm{Re}\lambda > 0$ the spectrum function is defined by the expression

$$\Lambda_1(\lambda, \kappa_\alpha, \alpha) = 1 + (1+\kappa_\alpha) K_\alpha^c \pi \int_{\mathbb{R}} \frac{F_\alpha^{(1)}(p)}{p - i\lambda} dp.$$

For $\mathrm{Re}\lambda \leqslant 0$, the integration contour for p is deformed from $\mathbb{R}$ to L as in Fig. 12, in order to avoid the singularity at $p = i\lambda$; the final result is (16).

The Taylor expansion of $\Lambda_1(\lambda, \kappa_\alpha, \alpha)$ is

$$\Lambda_1(\lambda, \kappa_\alpha, \alpha) = \sum_{k=0}^{\infty} \frac{\lambda^k}{k!} \frac{\partial^k \Lambda_1}{\partial \lambda^k}(0, \kappa_\alpha, \alpha), \tag{A1}$$

where

$$\frac{\partial^k \Lambda_1}{\partial \lambda^k}(\lambda, \kappa_\alpha, \alpha) = i^k (1+\kappa_\alpha) K_\alpha^c \pi \int_{\mathbb{R}} \frac{F_\alpha^{(k+1)}(p)}{p - i\lambda} dp. \tag{A2}$$

Performing the analytic continuation, we have

$$\begin{aligned}
\frac{\partial \Lambda_1}{\partial \lambda}(0, \kappa_\alpha, \alpha) &= -(1+\kappa_\alpha) K_\alpha^c \pi^2 F_\alpha^{(2)}(0), \\
\frac{\partial^2 \Lambda_1}{\partial \lambda^2}(0, \kappa_\alpha, \alpha) &= -(1+\kappa_\alpha) K_\alpha^c \pi \int_{\mathbb{R}} \frac{F_\alpha^{(3)}(p)}{p} dp, \\
\frac{\partial^3 \Lambda_1}{\partial \lambda^3}(0, \kappa_\alpha, \alpha) &= (1+\kappa_\alpha) K_\alpha^c \pi^2 F_\alpha^{(4)}(0).
\end{aligned} \tag{A3}$$

The first derivative with the definition $\alpha = F_\alpha^{(2)}(0)$ provides the coefficient b_α and the second and third derivatives directly give the coefficients c_α and d_α, respectively.

The constant term a_α satisfies

$$\Lambda_1(0, \kappa_\alpha, \alpha) = -(1+\kappa_\alpha) a_\alpha. \tag{A4}$$

Using the definition

$$\Lambda_1(0, 0, \alpha) = 1 + K_\alpha^c \pi \int_{\mathbb{R}} \frac{F_\alpha^{(1)}(p)}{p} dp, \tag{A5}$$

we can modify $\Lambda_1(0, \kappa_\alpha, \alpha)$ as

$$\Lambda_1(0, \kappa_\alpha, \alpha) = 1 + (1+\kappa_\alpha)[\Lambda_1(0, 0, \alpha) - 1]. \tag{A6}$$

This modification gives the coefficient a_α of (18).

2. Spectrum function at the origin

We consider the spectrum function at $\lambda = 0$:

$$\Lambda_1(0, \kappa_\alpha, \alpha) = 1 + (1+\kappa_\alpha) K_\alpha^c \pi \int_{\mathbb{R}} \frac{F_\alpha^{(1)}(p)}{p} dp. \tag{A7}$$

We show (19) under the assumption $c_\alpha > 0$.

We start from the case $\alpha \leqslant 0$. At the critical point $\kappa_\alpha = 0$, a purely imaginary critical eigenvalue $i\lambda_\mathrm{I}$ (embedded in the continuous spectrum) satisfies

$$1 + K_\alpha^c \pi \left(\mathrm{P} \int_{\mathbb{R}} \frac{F_\alpha^{(1)}(p)}{p + \lambda_\mathrm{I}} + i\pi F_\alpha^{(1)}(-\lambda_\mathrm{I}) \right) = 0. \tag{A8}$$

Considering the imaginary part of the above equation, we see that the unimodality of F_α implies that $\lambda_\mathrm{I} = 0$. Considering the real part, we then conclude that $\Lambda_1(0, 0, \alpha) = 0$.

We now turn to the case $\alpha > 0$. We may assume that $|\lambda_\mathrm{I}|$ is small for small $\alpha > 0$. We then have the expansion

$$\begin{aligned}
\mathrm{P} \int_{\mathbb{R}} \frac{F_\alpha^{(1)}(p)}{p + \lambda_\mathrm{I}} dp &= \mathrm{P} \int_{\mathbb{R}} \frac{F_\alpha^{(1)}(p - \lambda_\mathrm{I})}{p} dp \\
&= \int_{\mathbb{R}} \frac{F_\alpha^{(1)}(p)}{p} dp + \frac{\lambda_\mathrm{I}^2}{2} \int_{\mathbb{R}} \frac{F_\alpha^{(3)}(p)}{p} dp \\
&\quad + O(|\lambda_\mathrm{I}|^4).
\end{aligned} \tag{A9}$$

The above relation induces, for $\alpha > 0$ small,

$$\begin{aligned}
\Lambda_1(0, 0, \alpha) &= 1 + K_\alpha^c \pi \int_{\mathbb{R}} \frac{F_\alpha^{(1)}(p)}{p} dp \\
&> 1 + K_\alpha^c \pi \, \mathrm{P} \int_{\mathbb{R}} \frac{F_\alpha^{(1)}(p)}{p + \lambda_\mathrm{I}} dp = 0
\end{aligned} \tag{A10}$$

under the assumption $c_\alpha > 0$.

3. Positiveness of the coefficient c_α

We show that the coefficient is positive at $\alpha = 0$, namely, $c_0 > 0$ for the family (13). Then continuity with respect to α implies that c_α is positive around $\alpha = 0$.

The reference function at $\alpha = 0$ is

$$F_0(p) = C e^{-(\beta_4 p^2/2)^2}, \tag{A11}$$

where the normalization factor C is

$$C = \frac{1}{4\pi} \frac{1}{\int_0^\infty e^{-(\beta_4 p^2/2)^2} dp} = \left(\frac{\beta_4}{2} \right)^{1/2} \frac{1}{\pi \Gamma(1/4)} \tag{A12}$$

and $\Gamma(z)$ is the gamma function

$$\Gamma(z) = \int_0^\infty t^{z-1} e^{-t} dt. \tag{A13}$$

The third-order derivative of $F_0(p)$ is

$$F_0^{(3)}(p) = -C\beta_4^2 p\big(\beta_4^4 p^8 - 9\beta_4^2 p^4 + 6\big)e^{-(\beta_4 p^2/2)^2} \tag{A14}$$

and the coefficient c_0 is

$$\begin{aligned} c_0 &= K_\alpha^c \pi C \beta_4^2 \int_0^\infty \big(\beta_4^4 p^8 - 9\beta_4^2 p^4 + 6\big)e^{-(\beta_4 p^2/2)^2} dp \\ &= \frac{K_\alpha^c \beta_4^2}{2} \frac{8\Gamma(9/4) - 18\Gamma(5/4) + 6\Gamma(1/4)}{\Gamma(1/4)} \\ &= \frac{K_\alpha^c \beta_4^2}{2} > 0, \end{aligned} \tag{A15}$$

where we use the relation

$$\Gamma(z+1) = z\Gamma(z). \tag{A16}$$

APPENDIX B: NONLINEAR ANALYSIS

1. Expansion of self-consistent equations

We first introduce in Appendix B 1 a the setting for a general model, i.e., a general interaction potential ϕ in (1) and (2); we then show the expanded self-consistent equations in Appendix B 1 b. A sketch of the expansion is given in Appendix B 1 c. The scaling of each term is discussed in Appendix B 1 d and of M_k in Appendix B 1 e.

a. Setting

We consider (1) and (2) with a general interaction potential ϕ, a model whose one-body potential is

$$V(q) = -\sum_{k=1}^{\infty} K_k M_k \cos(kq). \tag{B1}$$

The self-consistent equations (32) are

$$M_k = I_k(\boldsymbol{M}) \quad (k \in \mathbb{N}), \tag{B2}$$

where the function I_k is defined by

$$I_k(\boldsymbol{M}) = \iint_\mu \langle \cos(kq)\rangle_J F_\alpha(p) dq\, dp. \tag{B3}$$

We used the equality $dqdp = d\theta dJ$ and the definition of the angle average $\langle\cdot\rangle_J$. Note that the average $\langle\cos(kq)\rangle_J$ depends on the one-body potential $V(q)$ and on the magnetizations $\boldsymbol{M}$ accordingly.

We expand $I_k(\boldsymbol{M})$ into a power series of $\boldsymbol{M}$. The idea is to divide the phase space μ into the two regions

$$U_1 = \{(q,p) \mid |p| < p_*\}, \quad U_2 = \{(q,p) \mid |p| > p_*\}, \tag{B4}$$

where $p_* > 0$ is a small value. In region U_1 we expand $F_\alpha(p)$ in a Taylor series

$$F_\alpha(p) = \sum_{n=0}^{\infty} F_\alpha^{(2n)}(0)\frac{p^{2n}}{(2n)!}, \quad (q,p) \in U_1. \tag{B5}$$

In region U_2 we expand $\langle\cos(kq)\rangle_J$ as

$$\langle\cos(kq)\rangle_J = \sum_{n=1}^{\infty} \frac{c_{k,n}(q;\boldsymbol{M})}{p^{2n}}, \quad (q,p) \in U_2. \tag{B6}$$

The expansion (B6) is based on symmetry between p and $-p$, and the convergence $\langle\cos(kq)\rangle_J \to 0$ when $|p| \to \infty$.

TABLE I. Contribution of the terms $T_{k,l}$ ($l = 1, \ldots, 5$) to I_k. See the text for the definitions of the symbols.

Region	U_1	U_2
$I_{k,n}$	$T_{k,2}$	$T_{k,2}$
$J_{k,n}$	$T_{k,1}, T_{k,3}, T_{k,4}$	$T_{k,5}$

b. Result

The expanded $I_k(\boldsymbol{M})$ is

$$I_k(\boldsymbol{M}) = \sum_{n=1}^{\infty}[I_{k,n}(\boldsymbol{M}) + J_{k,n}(\boldsymbol{M})], \tag{B7}$$

where

$$I_{k,n} = \frac{1}{(2n-1)!}\int_{-\pi}^{\pi} c_{k,n}(q;\boldsymbol{M})dq \int_{-\infty}^{\infty} \frac{F_\alpha^{(2n-1)}(p)}{p} dp \tag{B8}$$

and

$$J_{k,n} = \frac{F_\alpha^{(2n)}(0)}{(2n)!}\iint_\mu p^{2n}\left(\langle\cos(kq)\rangle_J - \sum_{l=1}^{n}\frac{c_{k,l}(q;\boldsymbol{M})}{p^{2l}}\right)dq\, dp. \tag{B9}$$

The scalings of $I_{k,n}$ and $J_{k,n}$ are $I_{k,n} = O(\|\boldsymbol{M}\|^n)$ and $J_{k,n} = O(\|\boldsymbol{M}\|^{n+1/2})$, respectively.

c. Sketch of expansion

The expansion (B5) in U_1 gives the contribution

$$T_{k,1} = \sum_{n=0}^{\infty}\frac{F_\alpha^{(2n)}(0)}{(2n)!}\iint_{U_1} p^{2n}\langle\cos kq\rangle dq\, dp \tag{B10}$$

to I_k. In U_2 with the expansion (B6), we have the function $F_\alpha(p)/p^{2n}$ in the integrand and we repeat the integration by parts to reduce the power of the denominator:

$$\begin{aligned} \int_{p_*}^{\infty}\frac{F_\alpha}{p^{2n}}dp = \frac{1}{(2n-1)!}\Bigg(&\int_0^{\infty}\frac{F_\alpha^{(2n-1)}(p)}{p}dp \\ &- \int_0^{p_*}\frac{F_\alpha^{(2n-1)}(p)}{p}dp \\ &+ \sum_{l=0}^{2n-2}(2n-2-l)!\frac{F_\alpha^{(l)}(p_*)}{p_*^{2n-1-l}}\Bigg). \end{aligned} \tag{B11}$$

The contribution from the first term is denoted by $T_{k,2}$. We expand $F_\alpha^{(2n-1)}(p)$ in the second term into a Taylor series and denote the contribution by $T_{k,3}$. In the third term, we expand $F_\alpha^{(l)}(p_*)$ into a Taylor series and use the trick

$$p_*^{2m+1} = \begin{cases} (2m+1)\int_0^{p_*} p^{2m}dp & (m \geqslant 0) \\ -(2m+1)\int_{p_*}^{\infty} p^{2m}dp & (m < 0). \end{cases} \tag{B12}$$

The contribution from the non-negative power terms is denoted by $T_{k,4}$ and from the negative power terms by $T_{k,5}$. All together, we have the expansion (B7). The contributions of the terms $T_{k,l}$ ($l = 1, \ldots, 5$) to I_k in regions U_1 and U_2 are summarized in Table I.

d. Scalings of $I_{k,n}$ and $J_{k,n}$

We first estimate the scaling of $c_{k,n}$ defined in (B6) by using the explicit form of $\langle\cos(kq)\rangle_J$ for energy $h(J)$:

$$\langle\cos(kq)\rangle_J = \int_{-\pi}^{\pi} \frac{\cos(kq)}{\sqrt{h-V(q)}}dq \Big/ \int_{-\pi}^{\pi} \frac{dq}{\sqrt{h-V(q)}}. \tag{B13}$$

The integrations are performed on a fixed-J contour. When h is sufficiently large, we perform the expansion

$$\frac{1}{\sqrt{h-V(q)}} = \frac{1}{\sqrt{h}}\left(1+\frac{V(q)}{2h}+\frac{3}{8}\frac{V(q)^2}{h^2}+\cdots\right). \tag{B14}$$

The factor $h(J)$ can be outside the integral. After performing the integral, we expand $h = p^2/2 + V(q)$ in denominators as

$$\frac{1}{2h} = \frac{1}{p^2}\left(1-\frac{2V(q)}{p^2}+\cdots\right). \tag{B15}$$

These expansions give the explicit expressions of $c_{k,n}$ as

$$c_{k,1} = \frac{1}{2\pi}\int_{-\pi}^{\pi} V(q)\cos(kq)dq = -\frac{K_k M_k}{2},$$
$$c_{k,2}(q) = -V(q)c_{k,1} + \frac{3}{4\pi}\int_{-\pi}^{\pi} V(q)^2\cos(kq)dq. \tag{B16}$$

We have $c_{k,n} = O(V^n)$ and hence $c_{k,n} = O(\|\boldsymbol{M}\|^n)$. This scaling directly provides $I_{k,n} = O(\|\boldsymbol{M}\|^n)$.

We have to be careful to estimate $J_{k,n}$ owing to the term $\langle\cos(kq)\rangle_J$. The expansion (B6) is valid for large $|p|$ and the leading term of $J_{k,n}$ is not $c_{k,n+1} = O(\|\boldsymbol{M}\|^{n+1})$. The main contribution to $J_{k,n}$ comes from $\langle\cos(kq)\rangle_J$ around the separatrix (see, for example, Fig. 1 of Ref. [23]). The separatrix width in the p direction is estimated as $p_{\rm sep} = O(\sqrt{\|\boldsymbol{M}\|})$ from $h_{\rm sep} = p_{\rm sep}^2/2 + V(0)$, where the separatrix energy $h_{\rm sep}$ and the potential V are of $O(\|\boldsymbol{M}\|)$. This estimation provides the scaling $J_{k,n} = O(\|\boldsymbol{M}\|^{n+1/2})$, because, roughly speaking, $J_{k,n}$ is of $O(p_{\rm sep}^{2n+1})$. See also [43] for the scaling in a generalized kinetic term.

e. Scalings of M_k

The scaling of M_k is estimated by picking up the leading two terms of (B7). From $c_{k,1}$ (B16), the factor $I_{k,1}$ forms $\Lambda_k(0,\kappa_\alpha,\alpha)$ with the unity of the left-hand side of the self-consistent equation (B2). Thus, we have truncated self-consistent equations as

$$\Lambda_k(0,\kappa_\alpha,\alpha)M_k = J_{k,1}(\boldsymbol{M}) \quad (k\in\mathbb{N}). \tag{B17}$$

Recall that $J_{k,1}$ is proportional to $F_\alpha^{(2)}(0) = \alpha$ for any k [see (B9)]. The leading term of $J_{k,1}$ is then of $O(\alpha M_1^{3/2})$. For $k=1$, combining it with the scaling $\Lambda_1(0,\kappa_\alpha,\alpha) = O(\kappa_\alpha)$ (20), we have $M_1 = O(\kappa_\alpha^2/\alpha^2)$. For $k>1$, we use $\Lambda_k(0,\kappa_\alpha,\alpha) = O(1)$ since the kth mode is far from being critical due to (3) and hence $M_k = O(\alpha M_1^{3/2})$. Inputting the scaling of M_1, we also have $M_k = O(\kappa_\alpha^3/\alpha^2)$. See Fig. 10 for confirmation of these scalings with respect to κ_α.

In the HMF model, we have $I_{1,2} = 0$, since the constant second term of $c_{1,2}$ in (B16) is zero. The vanishing $I_{1,2}$ explains the absence of $O(M)$ in (35).

2. Negativeness of the coefficient L_3

We show that $L_3 < 0$ for $F_0(p)$ in the HMF model. The explicit form of L_3 in the HMF model is

$$L_3 = -\frac{5\pi}{192}\int_{\mathbb{R}} \frac{F_\alpha^{(5)}(p)}{p}dp, \tag{B18}$$

where the integral is well defined since $F^{(5)}(p)$ is of $O(p)$. The fifth-order derivative of $F_0(p)$ is

$$F_0^{(5)}(p) = -C\beta_4^4 p\left(\beta_4^6 p^{14} - 30\beta_4^4 p^{10} + 195\beta_4^2 p^6 - 210p^2\right) \times e^{-(\beta_4 p^2/2)^2}. \tag{B19}$$

Straightforward computations give

$$L_3 = -\frac{5\beta_4^3}{8}\frac{\Gamma(3/4)}{\Gamma(1/4)} < 0. \tag{B20}$$

APPENDIX C: UNSTABLE MANIFOLD EXPANSION

The idea is to set up a series expansion in powers of the amplitude of the perturbation and to solve it order by order by projecting the full dynamics onto the unstable manifold instead of projecting onto the central manifold as usually done; one obtains in the end a reduced equation for the amplitude, which is singular at the bifurcation point. However, it is well defined away from the bifurcation point, at variance with standard central manifold computations. By construction, it is restricted to the unstable side of the bifurcation. According to the study of the linearized Vlasov operator in Sec. III, in the unimodal $\alpha \leqslant 0$ case, the unstable manifold is two dimensional, whereas it is four dimensional in the bimodal $\alpha > 0$ case. We restrict our discussion here to the unimodal case, in which the Landau pole moves on the real axis around the critical point (see Fig. 3).

The tangent space to the unstable manifold at the reference stationary state is spanned by the two eigenfunctions Φ and Φ^*; we expand f into

$$f(q,p,t) = F_\alpha(p) + g(q,p,t),$$

where

$$g(q,p,t) = A(t)\Phi(q,p) + A^*(t)\Phi^*(q,p) + S(q,p,A,A^*,t), \tag{C1}$$

with S of $O(|A|^2)$. The equation for the amplitude A is

$$\frac{dA}{dt} = \psi(A), \tag{C2}$$

where

$$\psi(A) = \lambda A + c_3(\lambda)A|A|^2 + O(|A|^5) \tag{C3}$$

on the unstable side of the critical point, namely, for $0<\lambda\ll 1$. The coefficient c_3 is

$$c_3(\lambda) = -\left(\frac{\pi K}{2}\right)^2 \tilde{c}_3(\lambda) \tag{C4}$$

and

$$\tilde{c}_3(\lambda) = \frac{1}{\lambda^3} - \frac{1}{\lambda^2}\frac{\Lambda_1^{(2)}(\lambda)}{\Lambda_1^{(1)}(\lambda)} + \frac{2}{3\lambda}\frac{\Lambda_1^{(3)}(\lambda)}{\Lambda_1^{(1)}(\lambda)} - \frac{1}{4}\frac{\Lambda_1^{(4)}(\lambda)}{\Lambda_1^{(1)}(\lambda)} + \frac{K_2}{K}\Lambda_1^{(2)}(\lambda)\left[-\frac{1}{\lambda}\left(1+\frac{K_2}{K}\frac{1}{\Lambda_2(2\lambda)}\right) + \frac{1}{2}\frac{1}{\Lambda_2(2\lambda)}\frac{\Lambda_1^{(2)}(\lambda)}{\Lambda_1^{(1)}(\lambda)}\right]. \tag{C5}$$

Here we omit the arguments κ_α and α in Λ_1 and derivatives are performed with respect to λ. We find a small real solution $|A|$ to the equation $\psi(A) = 0$ if $c_3 < 0$, while there is no small real solution if $c_3 > 0$. The bifurcation is hence continuous if $\tilde{c}_3(0) > 0$ and discontinuous if $\tilde{c}_3(0) < 0$.

The leading term of $\tilde{c}_3$ is positive $1/\lambda^3$ when $\alpha < 0$; hence the bifurcation is continuous [8,9]. However, the leading singularity of $\tilde{c}_3$ changes when $\alpha = 0$ since $\Lambda^{(1)}(\lambda) = O(\lambda)$ from

$$\Lambda_1^{(1)}(0, \kappa_\alpha, 0) = -(1+\kappa_\alpha)K_\alpha^c \pi^2 \alpha = 0. \tag{C6}$$

With the aid of the Taylor expansions of $\Lambda_1^{(1)}(\lambda, \kappa_\alpha, \alpha)$ and $\Lambda_1^{(2)}(\lambda, \kappa_\alpha, \alpha)$ around $\lambda = 0$, the leading singularity at $\alpha = 0$ is

$$\tilde{c}_3 \simeq \frac{1}{6\lambda^2}\frac{\Lambda_1^{(3)}(0)}{\Lambda_1^{(2)}(0)} = -\frac{1}{12\lambda^2}\frac{\pi F_0^{(4)}(0)}{\int_{\mathbb{R}} \frac{F_0^{(1)}(p)}{p^3} dp}. \tag{C7}$$

Since the function $F_0^{(1)}(p)$ is of $O(p^3)$ around $p = 0$, the integral in the denominator is well defined. In (C7), unimodality for $\alpha \leqslant 0$ implies that the numerator and the denominator are negative; hence the bifurcation is discontinuous from $\tilde{c}_3 < 0$. We also see from (C5) and (C7) that if $F_\alpha^{(2)}(0)$ is negative but small, the sign of $\tilde{c}_3$ will change from positive to negative as λ is increased from 0 (the critical point) to some small positive value. We then expect a continuous bifurcation with trapping scaling, followed by a jump in the saturated amplitude as the distance from the instability threshold is increased: This provides a qualitative understanding of Fig. 1 (when $\alpha < 0$). We also remark that the second Fourier coefficient of the coupling function ϕ [see (2)] does not affect the $\tilde{c}_3$ factor at $O(1/\lambda^2)$.

APPENDIX D: DISCONTINUITY OF BIFURCATION FOR HIGHER-ORDER FLATNESS

At the point $\alpha = 0$, the reference state is further classified by its leading order at $p = 0$. We defined that the reference state $F(p)$ is of order n when the Taylor expansion is

$$F(p) - F(0) = -bp^{2n} + O(p^{2(n+1)}). \tag{D1}$$

We will show now that for F of order 3 or higher ($n \geqslant 3$), the self-consistent equation predicts that the bifurcation is discontinuous.

If the order of F is 3 or higher, we have $F^{(2)}(0) = F^{(4)}(0) = 0$ and hence $L_{3/2} = L_{5/2} = 0$, since $L_{3/2}$ and $L_{5/2}$ are extracted from $J_{1,1} \propto F^{(2)}(0)$ and $J_{1,2} \propto F^{(4)}(0)$, respectively [see (B9) and the following scaling of $J_{k,n}$]. The leading term of $\varphi(M)$ [Eq. (35)] is therefore L_3, which is

$$L_3 = -\frac{5\pi}{192}\int_{\mathbb{R}} \frac{F^{(5)}(p)}{p} dp. \tag{D2}$$

The integration is well defined since $F^{(5)}$ is of $O(p)$ around $p = 0$. Under the conditions $F^{(2)}(0) = F^{(4)}(0) = 0$, we can derive another expression of L_3 as

$$L_3 = -\frac{5\pi}{192} 4! \int_{\mathbb{R}} \frac{F^{(1)}(p)}{p^5} dp \tag{D3}$$

by repeating integration by parts, where the integral is well defined since $F^{(1)}$ is of $O(p^5)$ around $p = 0$. Therefore, we have $L_3 > 0$ for a unimodal F, and the self-consistent equation $\Lambda_1(0, \kappa_0, 0) = L_3 M^2$ concludes that the bifurcation is discontinuous since $\Lambda_1(0, \kappa_0, 0) < 0$ in the unstable side $\kappa_0 > 0$ [see (20)]. We must not confuse $L_3 < 0$ shown in Appendix B 2 with $L_3 > 0$ found here, since the former (negative sign) is obtained for $F^{(2)}(0) = 0$ but $F^{(4)}(0) < 0$, while the latter (positive sign) is for $F^{(2)}(0) = F^{(4)}(0) = 0$. In general, L_3 is not zero however high the order of F is; hence the self-consistent equation predicts a discontinuous bifurcation for any F of order 3 or higher.

APPENDIX E: PREFACTORS OF SCALING RELATIONS FOR $\alpha \leqslant 0$

We compute here the eigenvalue collision point $\kappa_\alpha^{\rm col}$ and the jump point $\kappa_\alpha^{\rm J}$ for the family (13). The theoretically obtained prefactors are used in Fig. 9.

The eigenvalue collision point $\kappa_\alpha^{\rm col}$ satisfies

$$\frac{\kappa_\alpha^{\rm col}}{1+\kappa_\alpha^{\rm col}} = -\frac{b_\alpha^2}{4c_\alpha}. \tag{E1}$$

Recalling $b_\alpha = K_\alpha^c \pi^2 \alpha$, we have, at leading order in α,

$$\kappa_\alpha^{\rm col} = -\frac{\left(K_0^c \pi^2\right)^2}{4c_0}\alpha^2. \tag{E2}$$

Substituting the factor c_0 (A15), the eigenvalue collision point is estimated as

$$\kappa_\alpha^{\rm col} = -\frac{K_0^c \pi^4}{2\beta_4^2}\alpha^2. \tag{E3}$$

The values $\beta_4 = 3$ and $K_0^c \simeq 0.986\,225$ give

$$\kappa_\alpha^{\rm col} \simeq -5.34\alpha^2. \tag{E4}$$

The jump point $\kappa_\alpha^{\rm J}$ is

$$\kappa_\alpha^{\rm J} \simeq \frac{2(\tilde{L}_{3/2})^{3/2}}{3\left[3\tilde{L}_{5/2}F_0^{(4)}(0)\right]^{1/2}}|\alpha|^{3/2} \tag{E5}$$

at leading order. We have

$$F_0^{(4)}(0) = -6C\beta_4^2 = -\frac{6\beta_4^{5/2}}{\sqrt{2}\pi\Gamma(1/4)} \simeq -5.806\,42. \tag{E6}$$

Therefore, using (37), we have

$$\kappa_\alpha^{\rm J} \simeq 6.29|\alpha|^{3/2}. \tag{E7}$$

[1] P. J. Morrison, Hamiltonian and action principle formulations of plasma physics, Phys. Plasmas **12**, 058102 (2005).

[2] A. A. Vlasov, On vibration properties of electron gas, J. Exp. Theor. Phys. **8**, 291 (1938).

[3] L. Landau, On the vibrations of the electronic plasma, J. Phys. USSR **10**, 25 (1946).

[4] T. M. O'Neil, J. H. Winfrey, and J. H. Malmberg, Nonlinear interaction of a small cold beam and a plasma, Phys. Fluids **14**, 1204 (1971).

[5] D. del-Castillo-Negrete, Nonlinear evolution of perturbation in marginally stable plasmas, Phys. Lett. A **241**, 99 (1998).

[6] Y. Elskens and D. Escande, *Microscopic Dynamics of Plasmas and Chaos* (Institute of Physics, Bristol, 2003).

[7] N. J. Balmforth, P. J. Morrison, and J.-L. Thiffeault, Pattern formation in Hamiltonian systems with continuous spectra; a normal-form single-wave model, arXiv:1303.0065.

[8] J. D. Crawford, Universal Trapping Scaling on the Unstable Manifold for a Collisionless Electrostatic Mode, Phys. Rev. Lett. **73**, 656 (1994).

[9] J. D. Crawford, Amplitude equations for electrostatic waves: Universal singular behavior in the limit of weak instability, Phys. Plasmas **2**, 97 (1995).

[10] N. J. Balmforth, A. Roy, and C. P. Caulfield, Dynamics of vorticity defects in stratified shear flow, J. Fluid Mech. **694**, 292 (2012).

[11] S. Wiggins, *Introduction to Applied Nonlinear Dynamical Systems and Chaos*, 2nd ed. (Springer, New York, 2003).

[12] A. Antoniazzi, D. Fanelli, S. Ruffo, and Y. Y. Yamaguchi, Nonequilibrium Tricritical Point in a System with Long-Range Interactions, Phys. Rev. Lett. **99**, 040601 (2007).

[13] P. L. Palmer, J. Papaloizou, and A. J. Allen, Neighbouring equilibria to radially anisotropic spheres: Possible end-states for violently relaxed stellar systems, Mon. Not. R. Astron. Soc. **246**, 415 (1990).

[14] J. Barré, D. Métivier, and Y. Y. Yamaguchi, Trapping scaling for bifurcations in the Vlasov systems, Phys. Rev. E **93**, 042207 (2016).

[15] J. Barré, D. Métivier, and Y. Y. Yamaguchi, Towards a classification of bifurcations in Vlasov equations, Phys. Rev. E **102**, 052208 (2020).

[16] D. Porras and J. I. Cirac, Effective Quantum Spin Systems with Trapped Ions, Phys. Rev. Lett. **92**, 207901 (2004).

[17] K. Kim, M.-S. Chang, R. Islam, S. Korenblit, L.-M. Duan, and C. Monroe, Entanglement and Tunable Spin-Spin Couplings between Trapped Ions Using Multiple Transverse Modes, Phys. Rev. Lett. **103**, 120502 (2009).

[18] J. W. Britton, B. C. Sawyer, A. C. Keith, C.-C. J. Wang, J. K. Freericks, H. Uys, M. J. Biercuk, J. J. John, and J. Bollinger, Engineered two-dimensional Ising interactions in a trapped-ion quantum simulator with hundreds of spins, Nature (London) **484**, 489 (2012).

[19] R. Islam, C. Senko, W. C. Campbell, S. Korenblit, J. Smith, A. Lee, E. E. Edwards, C.-C. J. Wang, J. K. Freericks, and C. Monroe, Emergence and frustration of magnetism with variable-range interactions in a quantum simulator, Science **340**, 583 (2013).

[20] P. Richerme, Z.-X. Gong, A. Lee, C. Senko, J. Smith, M. Foss-Feig, S. Michalakis, A. V. Gorshkov, and C. Monroe, Non-local propagation of correlations in quantum systems with long-range interactions, Nature (London) **511**, 198 (2014).

[21] X. Leoncini, T. L. Van Den Berg, and D. Fanelli, Out-of-equilibrium solutions in the XY-Hamiltonian mean-field model, Europhys. Lett. **86**, 20002 (2009).

[22] P. de Buyl, D. Mukamel, and S. Ruffo, Self-consistent inhomogeneous steady states in Hamiltonian mean-field dynamics, Phys. Rev. E **84**, 061151 (2011).

[23] S. Ogawa and Y. Y. Yamaguchi, Nonlinear response for external field and perturbation in the Vlasov system, Phys. Rev. E **89**, 052114 (2014).

[24] S. Ogawa and Y. Y. Yamaguchi, Landau-like theory for universality of critical exponents in quasistationary states of isolated mean-field systems, Phys. Rev. E **91**, 062108 (2015).

[25] M. Tacu and D. Bénisti, Nonlinear adiabatic electron plasma waves: I. General theory and nonlinear frequency shift, Phys. Plasmas **29**, 052108 (2022).

[26] S. Inagaki and T. Konishi, Dynamical stability of a simple model similar to self-gravitating systems, Publ. Astron. Soc. Japan **45**, 733 (1993).

[27] M. Antoni and S. Ruffo, Clustering and relaxation in Hamiltonian long-range dynamics, Phys. Rev. E **52**, 2361 (1995).

[28] W. Braun and K. Hepp, The Vlasov dynamics and its fluctuations in the $1/N$ limit of interacting classical particles, Commun. Math. Phys. **56**, 101 (1977).

[29] R. L. Dobrushin, Vlasov equations, Funct. Anal. Appl. **13**, 115 (1979).

[30] H. Spohn, *Large Scale Dynamics of Interacting Particles* (Springer, Heidelberg, 1991).

[31] D. D. Holm, J. E. Marsden, T. Ratiu, and A. Weinstein, Nonlinear stability of fluid and plasma equilibria, Phys. Rep. **123**, 1 (1985).

[32] E. M. Lifshitz and L. P. Pitaevskii, *Course of Theoretical Physics* (Pergamon, Oxford, 1981), Vol. 10, Chap. 3.

[33] J. Binney and S. Tremaine, *Galactic Dynamics*, 2nd ed. (Princeton University Press, Princeton, 2008), Chap. 5.

[34] Y. Y. Yamaguchi and S. Ogawa, Conditions for predicting quasistationary states by rearrangement formula, Phys. Rev. E **92**, 042131 (2015).

[35] J. Barré, A. Olivetti, and Y. Y. Yamaguchi, Dynamics of perturbations around inhomogeneous backgrounds in the HMF model, J. Stat. Mech. (2010) P08002.

[36] J. Barré and Y. Y. Yamaguchi, Small traveling clusters in attractive and repulsive Hamiltonian mean-field models, Phys. Rev. E **79**, 036208 (2009).

[37] P. de Buyl, Numerical resolution of the Vlasov equation for the Hamiltonian mean-field model, Commun. Nonlinear Sci. Numer. Simulat. **15**, 2133 (2010).

[38] R. J. Briggs, J. D. Daugherty, and R. H. Levy, Role of Landau damping in crossed-field electron beams and inviscid shear flow, Phys. Fluids **13**, 421 (1970).

[39] R. L. Spencer and S. N. Rasband, Damped diocotron quasimodes of non-neutral plasmas and inviscid fluids, Phys. Plasmas **4**, 53 (1997).

[40] S. Ogawa, J. Barré, H. Morita, and Y. Y. Yamaguchi, Dynamical pattern formation in two-dimensional fluids and Landau pole bifurcation, Phys. Rev. E **89**, 063007 (2014).

[41] S. Schütz and G. Morigi, Prethermalization of Atoms Due to Photon-Mediated Long-Range Interactions, Phys. Rev. Lett. **113**, 203002 (2014).

[42] S. M. Churilov and I. G. Shukhman, Note on weakly nonlinear stability theory of a free mixing layer, Proc. R. Soc. London Ser. A **409**, 351 (1987).

[43] Y. Y. Yamaguchi, D. Das, and S. Gupta, Critical exponents in mean-field classical spin systems, Phys. Rev. E **100**, 032131 (2019).